The Plant Cell, Vol. 22: 1190–1215, April 2010, www.plantcell.org

Integrative Transcript and Metabolite Analysis of Nutritionally Enhanced *DE-ETIOLATED1* Downregulated Tomato Fruit [W]

Eugenia M.A. Enfissi,[a,b] Fredy Barneche,[c,d] Ikhlak Ahmed,[c] Christiane Lichtlé,[c] Christopher Gerrish,[a] Ryan P. McQuinn,[e] James J. Giovannoni,[e,f] Enrique Lopez-Juez,[a,b] Chris Bowler,[c] Peter M. Bramley,[a,b] and Paul D. Fraser[a,b,1]

[a] Centre for Systems and Synthetic Biology, University of London, Egham, Surrey TW20 0EX, United Kingdom
[b] School of Biological Sciences Royal Holloway, University of London, Egham, Surrey TW20 0EX, United Kingdom
[c] Institut de Biologie de l'Ecole Normale Supérieure, Centre National de la Recherche Scientifique, Unité Mixte de Recherche 8197, 75005 Paris, France
[d] Stazione Zoologica "Anton Dohrn," Villa Comunale, I 80121 Naples, Italy
[e] U.S. Department of Agriculture, Agricultural Research Service, Plant Soil and Nutrition Laboratory, Ithaca, New York 14853
[f] Boyce Thompson Institute for Plant Research, Cornell University Campus, Ithaca, New York 14853

Fruit-specific downregulation of the *DE-ETIOLATED1* (*DET1*) gene product results in tomato fruits (*Solanum lycopersicum*) containing enhanced nutritional antioxidants, with no detrimental effects on yield. In an attempt to further our understanding of how modulation of this gene leads to improved quality traits, detailed targeted and multilevel omic characterization has been performed. Metabolite profiling revealed quantitative increases in carotenoid, tocopherol, phenylpropanoids, flavonoids, and anthocyanidins. Qualitative differences could also be identified within the phenolics, including unique formation in fruit pericarp tissues. These changes resulted in increased total antioxidant content both in the polar and nonpolar fractions. Increased transcription of key biosynthetic genes is a likely mechanism producing elevated phenolic-based metabolites. By contrast, high levels of isoprenoids do not appear to result from transcriptional regulation but are more likely related to plastid-based parameters, such as increased plastid volume per cell. Parallel metabolomic and transcriptomic analyses reveal the widespread effects of *DET1* downregulation on diverse sectors of metabolism and sites of synthesis. Correlation analysis of transcripts and metabolites independently indicated strong coresponses within and between related pathways/processes. Interestingly, despite the fact that secondary metabolites were the most severely affected in ripe tomato fruit, our integrative analyses suggest that the coordinated activation of core metabolic processes in cell types amenable to plastid biogenesis is the main effect of *DET1* loss of function.

INTRODUCTION

Diets rich in fruits and vegetables have been associated with the reduced incidence of chronic disease states (Key et al., 2002). These findings have led many western governments to recommend the consumption of five portions of fruits and vegetables per day (Cooper, 2004). The health benefits conferred by certain fruits and vegetables have been attributed to the presence of health-promoting phytochemicals (more recently termed bioactives). Carotenoids, flavonoids, phenylpropanoids, tocopherols, and ascorbic acid (vitamin C) are all bioactives with potent antioxidant properties. Ripe tomato fruit (*Solanum lycopersicum*) contain significant amounts of these compounds and are the principal dietary source of the carotenoid lycopene in the human diet (Giovannucci, 2002).

The enhancement of nutritional quality is an important objective of modern plant breeding. Conventional molecular breeding and genetic modification (GM) technologies have been employed to generate better nutritional quality in crop plants, particularly tomato. Traditional genetic engineering of the target pathway has resulted in modest enhancement of specific metabolites, such as lycopene (Fraser et al., 2002) or flavonoids (Muir et al., 2001). Despite being more time consuming, labor intensive, and not as precise, non-GM approaches, such as marker-assisted screening, can be employed to achieve these increases (Zamir, 2001). In this way, consumer concerns associated with GM are avoided. However, more recently, genetic engineering approaches involving minipathway reconstruction in crop plants have resulted in dramatic increases in carotenoids, albeit in organs where endogenous levels are low (Ye et al., 2000; Diretto et al., 2007). The potential of transcription factors to modulate biochemical pathways has also been elegantly demonstrated recently (Butelli et al., 2008; Luo et al., 2008). In most cases, these approaches have focused on specific pathways to deliver a defined end product. By contrast, the manipulation of light signal transduction components (Liu et al., 2004; Davuluri, et al., 2005) or photoreceptors (Giliberto et al., 2005) in tomato fruit has facilitated enhancement of multiple bioactives

[1] Address correspondence to p.fraser@rhul.ac.uk.
The author responsible for distribution of materials integral to the findings presented in this article in accordance with the policy described in the Instructions for Authors (www.plantcell.org) is: Paul D. Fraser (p.fraser@rhul.ac.uk).
[W] Online version contains Web-only data.
www.plantcell.org/cgi/doi/10.1105/tpc.110.073866

simultaneously regardless of their formation by independent biosynthetic pathways (e.g., carotenoids and flavonoids). A disadvantage of manipulating components of the light signal transduction pathway, such as *DE-ETIOLATED1* (*DET1*; originally identified as *HIGH PIGMENT* [*hp2*]), *UV-DAMAGED DNA BINDING PROTEIN1* (*DDB1*; originally *hp1*), and *CULLIN-4* (Wang et al., 2008) either through transgenic constitutive expression or via mutant alleles such as $hp1^{w}$, *hp2*, $hp2^{j}$, and $hp2^{dg}$ is reduced fruit yield and loss of plant vigor (Davuluri et al., 2004). However, the fruit-specific downregulation of endogenous *DET1* expression is a good example of how light signal transduction components can be manipulated for biotechnological benefit without detrimental agronomic traits (Davuluri et al., 2005). These more recent examples of genetic modification offer important generic potential that is presently beyond the scope of conventional breeding.

Both the *DET1* and *DDB1* gene products are involved in the suppression of light responses in the absence of light. Their molecular function has been associated with chromatin remodeling (Benvenuto et al., 2002). Altered plastid biogenesis leading to an increased plastid compartment per cell is also believed to be a contributing factor to elevated chlorophyll and carotenoid levels in *hp* mutants. This evidence is based on the determination of plastid number per cell (Cookson et al., 2003; Liu et al., 2004) as well as an abundance of differentially expressed transcripts associated with plastid biogenesis (Kolotilin et al., 2007).

The fundamental characterization of *DET1* clearly points to a key role in core processes involved in plant development and environmental adaptation. However, in ripe tomato fruit, the downregulation of *DET1* results in the simultaneous elevation of secondary metabolites associated with nutritional quality. To provide an insight into the dynamic molecular events and metabolic reprogramming leading to this *DET1* fruit chemotype, we performed integrative transcriptomic and metabolomic analyses.

RESULTS

Phenotypic Stability and Correlation with *DET1* Downregulation during Fruit Development

Phenotypic inheritance has been shown for several *DET1* downregulated events in the second generation (T2); these lines were generated from segregating primary transformants (T1) (Davuluri et al., 2005). Selected lines representing three different fruit specific promoters (2A11, TFM7, and P119) have subsequently been taken through a further three generations (T3 to T5) in this study and their pheno/chemotypes evaluated. In comparison to their wild-type background (T56), all genotypes exhibited dark-green mature fruit and a more intense red internal coloration of the ripe fruit. Determination of the carotenoid content found in ripe fruit was consistently higher over the three generations (see Supplemental Table 1 online). Therefore, stable phenotypic inheritance has been achieved, leading to the designation of these lines as the 2A11, TFM7, and P119 varieties. In comparison to their T56 background, no observable differences were found in physiological parameters (e.g., fruit yield, diameter, rate of ripening, plant height, and growth rate) among the *DET1* varieties, in agreement with the determinations performed previously on a wider range of events (Davuluri et al., 2005). Material from these varieties has been used in this study for detailed characterization using multiple omics-based approaches.

The promoters 2A11, TFM7, and P119 are known to act during fruit development (Davuluri et al., 2005), but the precise timing and strength by which they control *DET1* expression remain poorly characterized. To determine the quantitative spatial timing of *DET1* downregulation by the three promoters, a developmental series of fruit was generated and qRT-PCR used to determine *DET1* expression levels. Seven stages from immature fruit to red-ripe as illustrated in Figure 1A have been analyzed. The 2A11 promoter was found to be the weakest of the three promoters; its effects were greatest in developmental stages 4 and 5 (Figure 1B) but represented only a 20% reduction in *DET1* expression compared with the wild type. After stage 5, endogenous *DET1* transcripts returned to wild-type levels. *DET1* expression was similar under both P119 and TFM7 promoter control. A reduction in the amount of *DET1* transcript was initially observed at stage 3 and progressed until stage 6 (mature green), when an approximate 70% reduction in *DET1* expression occurred in both the P119 and TFM7 varieties (Figure 1B). Curiously, in both cases, *DET1* expression returned to wild-type levels at the red-ripe stage.

In all cases, increases in chlorophyll, carotenoids, and phenolics were concurrent with the initiation of *DET1* downregulation and mimicked expression profiles until *DET1* downregulation was alleviated (Figures 1C to 1E). At this point, increased fruit carotenoid, chlorophyll, and phenolic contents were maintained even in the absence of *DET1* downregulation. On the basis of the expression and the concurrent appearance of the phenotype, detailed characterization was initiated at the mature green stages of fruit development (stage 5).

The Effect of *DET1* Downregulation on Carotenoid (Isoprenoid) and Phenolic Formation at the Metabolite and Gene Expression Level

Carotenoid/Isoprenoid Formation

Carotenoids, xanthophylls, chlorophylls, and tocopherols were profiled simultaneously during fruit development and ripening for all three *DET1* varieties. In comparison to fruits from the T56 wild type, chlorophyll levels were elevated in all *DET1* varieties up to the breaker stage (Table 1). The 2A11 variety showed a significant 3-fold increase in chlorophyll at the mature green stage of fruit development. In both the TFM7 and P119 varieties, greater increases (9-fold) in chlorophyll were evident, and the total carotenoid content of the fruit increased concurrently with chlorophyll content. As a result, the carotenoid to chlorophyll ratio (~3.0) between the *DET1* varieties remained constant and similar to the wild type. For comparison, two mutant *hp2* alleles in different backgrounds (Moneymaker and San Marzano) were also analyzed. The total carotenoid content of the mature green fruit were similar to the *DET1* varieties in these mutants (Table 1). However, the backgrounds for each of the *hp* alleles contained higher carotenoid contents; therefore, the relative increases in the P119 and TFM7 varieties were greater (e.g., 8-fold compared

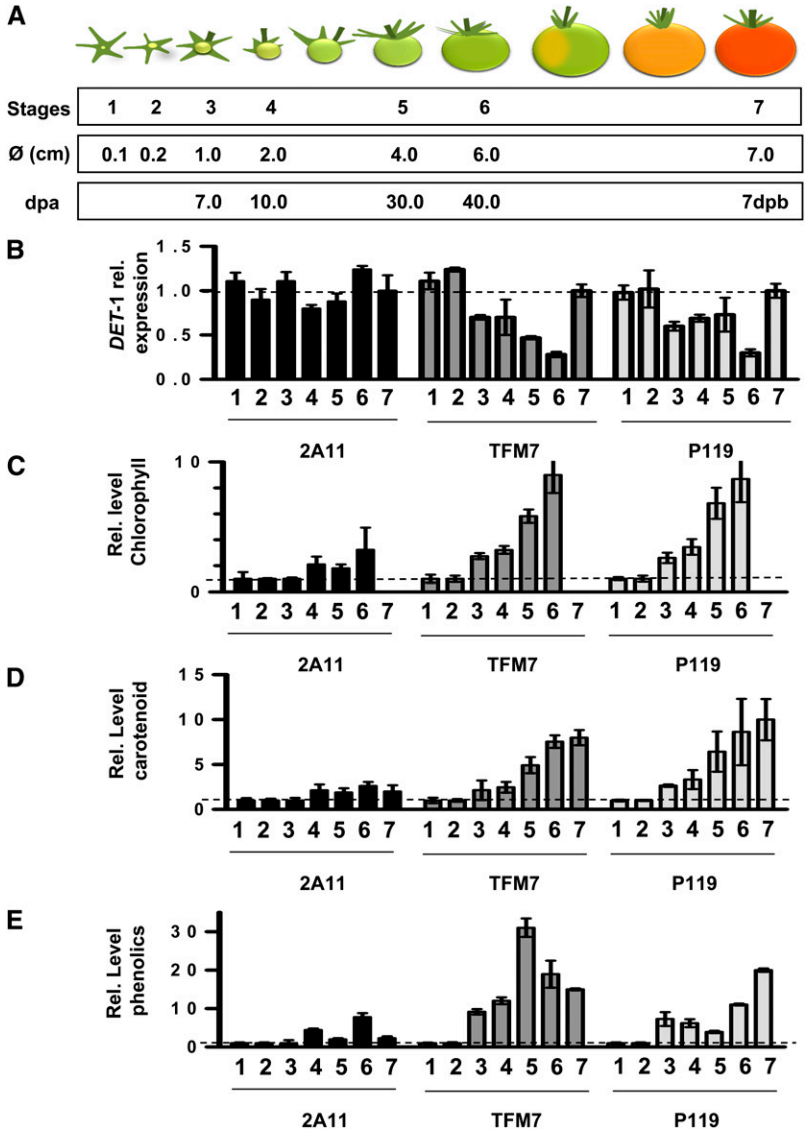

Figure 1. Profile of Relative *DET1* Expression, Total Chlorophyll, Carotenoid, and Phenolic Levels in the 2A11, TFM7, and P119 Genotypes during Fruit Development and Ripening.

(A) Illustration of the designated fruit stages sampled, their approximate diameter, days after anthesis (dpa), and days postbreaker (dpb).
(B) Relative changes in *DET1* expression (determined by qRT-PCR) among the *DET1* downregulated varieties compared with their control (T56) at the indicated stages of development and ripening. The dashed gray line designates a ratio of 1 (i.e., no change in expression).
(C) to **(E)** Relative changes in total chlorophyll, carotenoid, and phenolic contents compared with their controls. Phenolics are represented by the sum of the phenylpropanoids, flavonoids, and anthocyanins analyzed. Typical determinations (mg/g DW) for total chlorophylls, carotenoid, and phenolics found in the T56 at the various stages are 4.0, 1.1, and 1.0 at stage 3; 4.0, 1.0, and 0.9 at stage 4; 3.3, 0.8, and 0.63 at stage 5; 0.04, 0.02, and 0.2 at stage 6; and 0, 3.0, and 0.4 at the red-ripe stage (stage 7). Biological replicates were performed in triplicate and the data presented as means ± SD.

with 4-fold in the *hp* alleles). The effects of *DET1* on the individual carotenoids are also shown in Table 1. No change in the carotenoid composition was observed in the *DET1* and *hp* mutant varieties analyzed, with the relative increases among individual carotenoids being similar.

At the breaker stage of fruit ripening, the 2A11, TFM7, and P119 varieties showed 4-, 16-, and 13-fold increases, respectively, in total carotenoid content compared with the T56 background. These levels were far greater than those of the *hp* mutant alleles, which exhibited a 2-fold relative increase compared with their wild-type backgrounds. Table 1 documents the levels of individual carotenoids found in fruit at the breaker stage. The carotenoids lutein and β-carotene were predominant in both the T56 background and *DET1* varieties. Of the carotenes, phytoene was only found in the TFM7 and P119 varieties, and lycopene was only present in the 2A11 and TFM7 varieties, whereas

Table 1. Carotenoid, Chlorophyll, and Tocopherol Contents Found in the Transgenic DET1 Downregulated Varieties (2A11, TFM7, and P119) and hp2 Mutant Alleles Compared with Their Wild-Type Backgrounds

Isoprenoids (μg/g DW)	*DET1* Genotypes Mature Green							
	T56	2A11	TFM7	P119	MM	MM*hp2*^{j}	SM	SM*hp2*
Neoxanthin	1.5 ± 0.10	**4.6 ± 0.3** ***	**11.0 ± 0.3** ***	**11.9 ± 0.5** ***	2.3 ± 0.1	**8.2 ± 0.2** ***	2.4 ± 0.3	**10.3 ± 0.2** **
Violaxanthin	3.0 ± 0.03	**9.3 ± 0.3** ***	**29.5 ± 0.4** ***	**27.2 ± 1.0** ***	8.1 ± 0.1	**32.4 ± 0.6** ***	10.7 ± 0.1	**36.4 ± 0.8** ***
Lutein	7.7 ± 0.30	**18.7 ± 0.7** ***	**52.4 ± 1.0** ***	**65.4 ± 0.6** ***	17.8 ± 0.5	**53.1 ± 0.6** ***	19.4 ± 0.3	**73.5 ± 1.5** **
β-Carotene	4.0 ± 0.10	**9.6 ± 1.6** *	**29.0 ± 4.0** **	**35.1 ± 2.5** ***	11.2 ± 0.5	**25.3 ± 1.0** ***	7.6 ± 0.4	**31.6 ± 0.1** ***
Total carotenoid	16.2 ± 1.00	**42.2 ± 3.0** ***	**122.1 ± 5.0** ***	**140.0 ± 0.7** ***	39.4 ± 1.0	**119.0 ± 1.6** ***	40.0 ± 1.0	**151.7 ± 2.2** ***
Chlorophyll	43.7 ± 0.60	**141.2 ± 7.0** ***	**394.2 ± 12.0** ***	**381.1 ± 2.0** ***	97.4 ± 2.9	**328.4 ± 4.0** ***	119.2 ± 3.3	**459.1 ± 12.2** **
CHL:CAR	2.7	3.3	3.2	2.7	2.5	2.7	3.0	3.0
	DET1 Genotypes Breaker Fruit							
Isoprenoids (μg/g DW)	T56	2A11	TFM7	P119	MM	MM*hp2*^{j}	SM	SM*hp2*
Neoxanthin	1.3 ± 0.02	1.4 ± 0.3	1.4 ± 0.1	**9.7 ± 0.4** **	ND	**10.0 ± 0.3** ***	ND	**7.7 ± 4.0** ***
Violaxanthin	0.9 ± 0.02	**5.8 ± 1.5** ***	**8.4 ± 1.7** *	**35.6 ± 2.3** **	11.6 ± 5.6	**61.8 ± 5.2** **	19. 2 ± 1.3	**76.8 ± 1.3** ***
Lutein	2.1 ± 0.60	**7.7 ± 2.2** ***	**34.3 ± 6.0** **	**36.4 ± 3.0** ***	23.1 ± 1.6	**47.0 ± 1.3** ***	27.4 ± 0.5	**94.6 ± 1.5** ***
β-Carotene	9.7 ± 0.60	**28.2 ± 8.0** ***	**129.8 ± 24.0** **	**83.8 ± 5.5** ***	153.2 ± 18.0	188.4 ± 6.9	250.0 ± 7.7	**426.7 ± 11.0** ***
Lycopene	ND	**0.1 ± 0.0** ***	**10.2 ± 2.0** ***	ND	14.5 ± 2.7	ND	57.7 ± 2.0	18.9 ± 0.7
Neurosporene	2.04 ± 0.03	**6.20 ± 1.6** ***	**32.5 ± 3.4** *	**16.0 ± 0.8** **	29.8 ± 1.1	**41.2 ± 1.3** **	42.6 ± 0.20	**85.0 ± 6.2** **
Phytofluene	ND	ND	ND	ND	ND	ND	6.1 ± 0.23	1.6 ± 0.2
Phytoene	ND	ND	**1.7 ± 0.01** **	**4.6 ± 0.4** **	8.6 ± 0.33	0.4 ± 0.002	24.4 ± 0.3	5.2 ± 0.13
Total carotenoid	14.6 ± 2.7	**50.0 ± 14.0** ***	**217.1 ± 38.9** **	**182.9 ± 12.0** **	241.0 ± 23.0	**337.3 ± 13.7** *	442.6. ± 25.0	**714.0 ± 11.7** **
Chlorophyll	25.0 ± 2.0	**176.9 ± 24.0** ***	**127.4 ± 22.5** ***	**176.9 ± 24.0** ***	105.2 ± 9.5	**272.0 ± 23.0** **	88.9 ± 2.4	**462.1 ± 5.0** **
CHL:CAR	1.7	3.5	0.6	1.0	0.4	0.8	0.2	0.6
Tocopherols	19.2 ± 0.6	**37.0 ± 10.0** **	**176.3 ± 14.0** *	**86.6 ± 0.04** **	87.0 ± 9.3	**257.4 ± 6.2** **	163.7 ± 3.4	**433.6 ± 20.0** **
	DET1 Genotypes Ripe Fruit							
Isoprenoids (μg/g DW)	T56	2A11	TFM7	P119	MM	MM*hp2*^{j}	SM	SM*hp2*
Violaxanthin	3.0 ± 0.1	**5.5 ± 0.9** *	**9.5 ± 0.6** ***	**37.3 ± 09** ***	ND	**15.2 ± 0.6** ***	6.7 ± 0.2	**16.1 ± 0.2** ***
Lutein	13.5 ± 0.10	**24.8 ± 0.7** ***	**46.4 ± 0.8** ***	**132.4 ± 3.0** ***	19.3 ± 0.3	**70.8 ± 0.6** ***	19.4 ± 0.2	**68.04 ± 0.8** ***
β-Carotene	198.0 ± 3.0	28.2 ± 8.0	**851.1 ± 34.0** **	**1455.6 ± 39.6** ***	351.0 ± 18.0	188.4 ± 6.9	250.0 ± 7.7	**426.7 ± 11.0** ***
Lycopene	321.7 ± 4.5	**725.2 ± 14.3** ***	**955.5 ± 17.0** ***	**1574.7 ± 13.5** ***	483.5 ± 20.7	**1088.6 ± 14.0** ***	347.3 ± 4.6	**898.7 ± 11.0** ***
Neurosporene	3.4 ± 0.4	ND	ND	**48.6 ± 6.7** ***	ND	ND	ND	ND
Phytofluene	41.0 ± 1.8	**144.0 ± 7.0** ***	**68.2 ± 3.2** ***	**363.7 ± 3.2** ***	130.7 ± 1.0	**181.4 ± 4.0** ***	117.0 ± 1.5	**213.8 ± 7.9** ***
Phytoene	129.2 ± 0.4	**315.6 ± 5.2** *	**137.2 ± 1.9**	**583.4 ± 0.8** ***	302.6 ± 5.0	321.1 ± 2.4	292.2 ± 3.2	**363.6.2 ± 4.7** ***
Total carotenoid	708.4 ± 8.0	**1659.0 ± 42.0** ***	**2064.8 ± 44.5** ***	**4179.5 ± 21.0** ***	1287.2 ± 38.0	**2773.4 ± 37.0** ***	1347.0 ± 37.0	**2861.5 ± 59.0** ***
Tocopherols	148.1 ± 11.5	112.4 ± 15.3	**284.2 ± 6.1** ***	**505.1 ± 6.2** ***	76.2 ± 3.2	**403.8 ± 7.0** ***	94.7 ± 5.7	**258.3 ± 5.8** ***

Tomato fruit at different developmental and ripening stages have been analyzed: mature green, breaker, and ripe. Carotenoid, chlorophyll, and tocopherol contents are given as μg/g DW. Methods used for determinations are described in Methods. Three representative fruit from a minimum of three plants were used for each developmental/ripening stage. The fruit were pooled and at least three determinations made per sample, making a minimum of three biological and three technical replicates. The mean data are presented ± SD. Student's *t* tests were used to determine significant differences between respective wild-type backgrounds and transgenic varieties. $P < 0.05$, $P < 0.01$, and $P < 0.001$ are indicated by *, **, and ***, respectively. Values in bold indicate where significant differences have been found compared to the wild-type backgrounds. ND, not detected; CHL, chlorophyll; CAR, carotenoid; MM, Moneymaker; SM, San Marzano.

neurosporene was detected in all three varieties, showing 3-, 17-, and 8-fold increases in 2A11, TFM7, and P119, respectively. In addition to carotenoids, the 2A11, TFM7, and P119 varieties contained increased tocopherol (vitamin E) contents: up to 9-fold in the TFM7 variety. α-Tocopherol was the predominant tocopherol but with γ-tocopherol detectable and mimicking the relative changes in α-tocopherol.

Lycopene was the major carotenoid found in all ripe tomato fruit analyzed regardless of variety (Table 1). Increases in lycopene ranged from 2-fold in 2A11 to 5-fold increases in the *hp* mutant alleles. Phytoene and phytofluene both showed similar relative increases compared with their T56 background levels. In the 2A11 and TFM7 varieties, β-carotene levels were increased akin to the other carotenoids analyzed. However, in the P119 variety, the increase in β-carotene was significantly (Table 1) greater (7-fold), reaching 2.0 mg/g dry weight (DW), and represented the equivalent of 3.5 times the recommended daily allowance (RDA) of β-carotene (provitamin A) per tomato. Therefore, the RDA can be delivered in one P119 ripe tomato, instead of requiring a person to eat three tomatoes with typical β-carotene contents. Tocopherol contents in ripe fruit were elevated in both the TFM7 and P119 varieties up to 2- and 3-fold, respectively. The increases in tocopherols mean that the RDA for tocopherol can be achieved by consuming two P119 ripe

tomato fruits instead of six or seven T56 wild-type ripe tomatoes.

To ascertain the causative effect of DET1 on carotenoid and tocopherol levels, qRT-PCR was performed to determine if transcriptional upregulation of key carotenoid and tocopherol biosynthetic genes had occurred. The transcript levels for genes encoding carotenoid and tocopherol biosynthetic enzymes showed no consistent trend among the 2A11, TFM7, and P119 varieties (Figures 2A and 2B). In all three varieties, the majority of the pathway transcripts were not significantly affected compared with their control (T56) levels at the mature green stage of fruit development (Figure 2A). Notable relative increases over 2-fold included *PSY*-2 in both the P119 and 2A11 varieties, and *GGPPS*-2 and *LCY*-E in the P119 and TFM7 varieties, respectively. However, reductions in transcript levels were more predominant. For example, *DXS* transcripts were reduced at least 2-fold in both TFM7 and P119, and *PSY*-1 and *CYC*-B were lower in 2A11 and TFM7, whereas *LCY*-E was lower in both 2A11 and P119 (Figure 2A). Transcripts for tocopherol biosynthetic enzymes were elevated significantly at the mature green stage, for example, in P119, γ-methyl tocopherol transferase (*GMTT*) and geranylgeranyl pyrophosphate reductase (*GGPR*) were increased 8- and 5-fold, respectively.

In ripe fruit, most transcripts for carotenoid biosynthetic enzymes were either decreased or showed very similar levels relative to the control (T56) (Figure 2B). By contrast, several isoprenoid related transcripts, such as *GMTT* and *GGPPS*-2, were increased 5- and 10-fold in the P119 and 2A11 varieties, respectively. In the 2A11 variety, increases over 2-fold were observed for *DXS*, *ZDS*, and *LCY-B* transcripts. In spite of the overall increases in carotenoids and isoprenoids, the most striking observation from transcriptional analysis of the biosynthetic genes is therefore that no consistent trends existed among the varieties.

Phenylpropanoid, Flavonoid, and Anthocyanin Formation

Fruit samples were divided into skin and pericarp tissue and analysis performed on each tissue type (Table 2). In the skin tissue from control (T56) mature green fruit, the phenylpropanoids caffeic acid, *p*-coumaric, and chlorogenic acid were detected, together with flavonoid derivatives of quercetin. Dramatic increases in the levels of caffeic acid and quercetin derivatives were measured in the TFM7 and P119 varieties compared with their control (T56) (Table 2). For example, in the P119 variety, caffeic acid and quercetin showed a 13- and 5-fold elevation, respectively, compared with the control (T56). The trend of increased phenolics was also evident in the *high pigment* (*hp2*^{j}) mutant alleles (Table 2), although increases were not as great (e.g., a 2.5- to 8-fold increase in caffeic acid content was found in *hp2*^{j} [Moneymaker] compared with 13-fold in P119). The skin tissue from ripe fruit contained caffeic acid, *p*-coumaric acid, chlorogenic acid, quercetin derivatives, and naringenin-chalcone (Table 2). In all three varieties, naringenin-chalcone content was reduced (2- to 4-fold), while quercetin derivatives were increased (up to 4-fold). Chlorogenic acid contents were also elevated in all varieties, most notably in the TFM7 variety where a 7.5-fold increase was evident. In the P119 variety, the caffeic acid content was also elevated 13-fold in comparison to the control (T56). Interestingly, the *hp2*^{j} mutant alleles in both Moneymaker and San Marzano backgrounds all demonstrated increases (up to 10-fold) for all phenolics tested except naringenin-chalcone (Table 2).

In the pericarp tissue from control mature green fruit, caffeic acid was the only detectable phenolic, its content increasing 5- and 18-fold in the TFM7 and P119 varieties, respectively (Table 2). Quercetin derivatives were found in 2A11, TFM7, and P119, whereas chlorogenic acid was unique to TFM7 and P119, and *p*-coumaric acid was unique to P119. Similar findings were found with the *hp2* alleles in the backgrounds tested (Moneymaker and San Marzano), although the amounts determined were not as substantial as those found with the transgenic *DET1* genotypes (Table 2). Ripe pericarp tissue from the control (T56) variety contained all the phenylpropanoids targeted with the analytical system used, but no flavonoids (e.g., quercetin derivatives and naringenin-chalcone) (Table 2). Interestingly, in comparison to the T56 background where flavonoids were absent in the pericarp tissue, the presence of flavonoids in this tissue was found in both the TFM7 and P119 varieties. The *hp2* mutant alleles also contained flavonoids in the pericarp (Table 2). The caffeic, *p*-coumaric, and chlorogenic acid contents of the P119 variety were increased 3-fold in all cases. Chlorogenic acid content was also elevated in the TFM7 variety. In comparison, the *hp2* mutant alleles possessed similar increases in chlorogenic acid (3-fold), *p*-coumaric acid was not detected, and caffeic acid was elevated only in the *hp2*^{j} Moneymaker background.

The total content of anthocyanidins present in mature green fruit was increased for all *DET1* and *hp* mutant alleles (2- to 8-fold; Table 2). Anthocyanidin content in the ripe fruit was increased only in the *DET1* varieties (3- to 5-fold; Table 2). Analysis of the anthocyanidins present by liquid chromatography–tandem mass spectrometry revealed the sole presence of delphinidin-3-(coumaroyl)-rutinoside-5-glucoside ($M+H^+$ 919 *m/z*).

At the level of gene expression, several key transcripts relating to biosynthetic genes involved in phenylpropanoid, flavonoid, and anthocyanidin formation were quantified (Figures 3A and 3B). In both the mature green and ripe fruit, the levels of several transcripts encoding enzymatic steps within these phenolic pathways were dramatically increased (e.g., *CHS* up to 37.5-fold), but there was no unifying trend between the different varieties with respect to the biosynthetic steps they affect or the stage of fruit development/ripening at which the effects become evident. For example, *CHS* transcripts in mature green fruit were increased 37-fold in P119 but only increased 2-fold in TFM7 and were reduced in 2A11. By contrast, *CHS* transcripts in the ripe stage increased 14-fold in TFM7 but increased only a modest 3-fold in P119. Increased *F3H* and *FLS* transcripts were found only in TFM7 at the ripe stage. Other notable increases mainly occurred in the P119 variety and were related to anthocyanidin biosynthetic transcripts (e.g., *DFR*, *ANS*, *RT*, and *3-GT* were induced 5- to 35-fold) (Figures 3A and 3B). In spite of these inconsistencies, a general trend of increased expression of genes involved in phenylpropanoid, flavonoid, and anthocyanidin biosynthesis was nonetheless more evident than it was for the carotenoid/isoprenoid genes (cf. Figures 2 and 3).

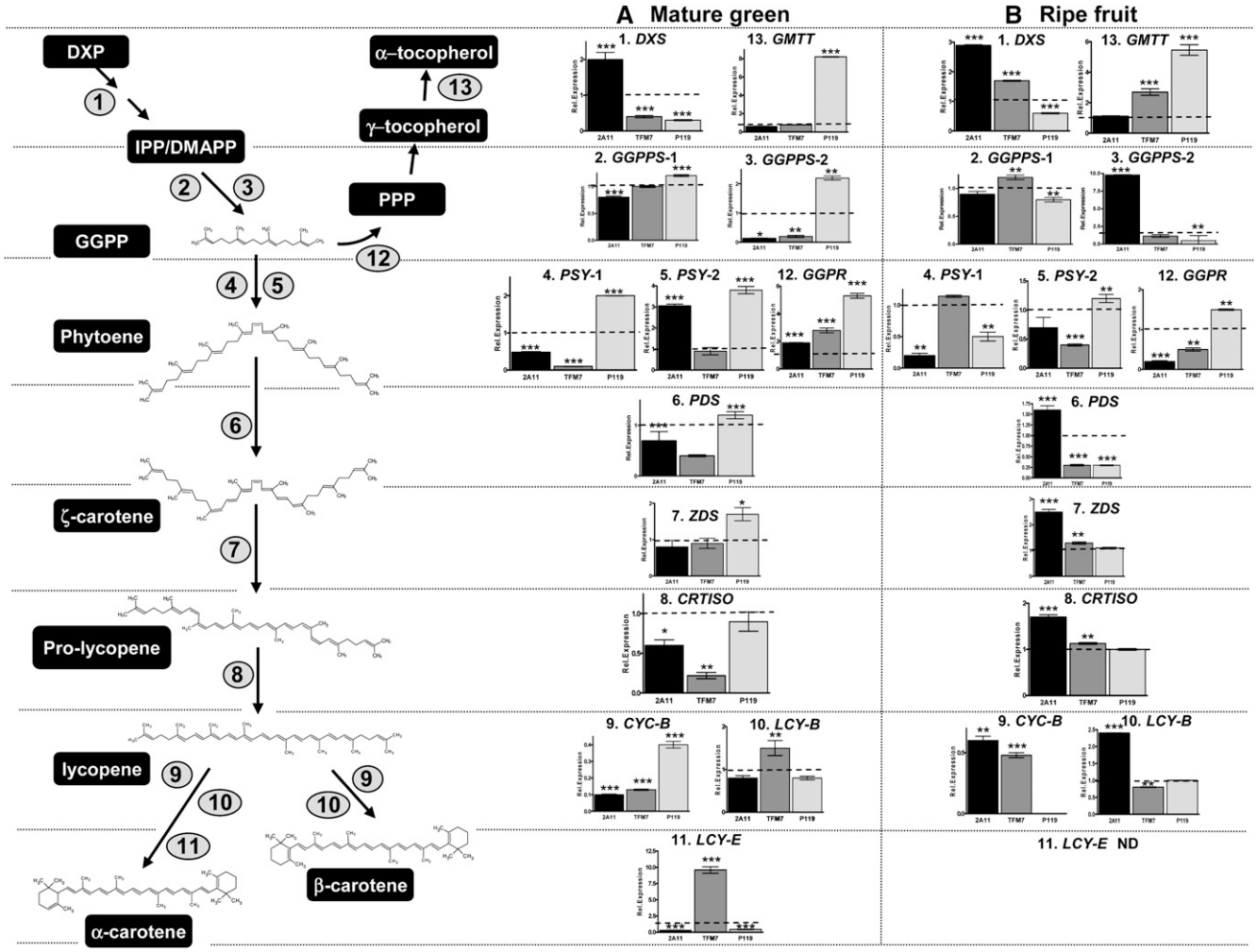

Figure 2. The Effect of *DET1* Downregulation on Carotenoid/Isoprenoid-Related Gene Expression Levels in Mature Green and Ripe Fruit.

Pooled fruit originating from three plants per promoter (2A11, TFM7, and P119) were pulverized into a homogenous powder as described in Methods. Total RNA was then extracted from an aliquot of this material. qRT-PCR was performed with gene-specific primers for (1) *DXS*, 1-deoxy-D-xylulose-5-phosphate synthase; (2) *GGPPS-1*, 1-geranylgeranyl pyrophosphate synthase-1; (3) *GGPPS-2*; (4) *PSY*-1, phytoene synthase-1; (5) *PSY*-2; (6) *PDS*; (7) *ZDS*, ζ-carotene desaturase; (8) *CRTISO*, carotene isomerase; (9) *CYC-B*, β-lycopene cyclase; (10) *LCY-B*, β-lycopene cyclase; (11) *LCY-E*, ε-lycopene cyclase; (12) *GGPPR*, geranylgeranyl pyrophosphate reductase; and (13) *GMTT*. The locations of these enzymatic steps on the pathway are shown by the numbers superimposed into the circles with the gray backgrounds. The expression data shown have been normalized to the expression of actin. Data are represented as relative levels found in the three varieties compared with the T56 wild type. Statistical determinations are shown as mean ± SD values, where $n = 3$ to 6. Student's t tests illustrate statistically significant (*$P < 0.05$, **$P < 0.01$, and ***$P < 0.001$) differences from the wild-type levels. The black bars of the histogram indicate the levels in 2A11, gray bars TFM7, and pale gray P119. The dashed line across each histogram indicates the relative wild-type expression level. GGPP, geranylgeranyl pyrophosphate; PPP, phytyl pyrophosphate; IPP, isopentenyl pyrophosphate; DMAPP, dimethylally pyrophosphate. ND, not detectable.

Total Antioxidant Activities

To assess whether the increased levels of carotenoids and phenolics had resulted in elevated total antioxidant capacity in the *DET1* varieties, trolox-equivalent antioxidant capacity (TEAC) analysis was performed (see Supplemental Figure 1 online). Carotenoids are potent antioxidants that act in the nonpolar (hydrophobic) phase, whereas phenolics exert their effects in the polar extracts. Therefore, both polar and nonpolar extracts were subjected to TEAC assays. Increases in antioxidant capacity were found in nonpolar extracts prepared from all three varieties at the mature green stage (see Supplemental Figure 1A online) and the ripe stage (see Supplemental Figure 1B online). The 2A11 mature green fruit extracts demonstrate modest 2-fold increases, while extracts from the TFM7 and P119 varieties approach a 4-fold increase (see Supplemental Figure 1A online). Nonpolar ripe fruit extracts from the TFM7 and P119 varieties demonstrate increased (approaching 2-fold) antioxidant activity (see Supplemental Figure 1B online). Polar extracts prepared

Table 2. Phenolic Contents of the DET1 Downregulated Varieties Determined Both in Skin and Pericarp Tissues at the Mature Green and Ripe Stages of Fruit Development and Ripening; the Bottom Section Shows the Changes in Total Anthocyanin Content at Mature Green and Ripe Stages

	DET1 Genotypes Mature Green Skin							
Phenolics (μg/g DW)	T56	2A11	TFM7	P119	MM	MM*hp2*^{j}	SM	SM*hp2*
Caffeic acid	576 ± 40	**292 ± 14** **	**1,911 ± 178** **	**7,667 ± 460** ***	1,535 ± 57	**12,839 ± 634** ***	3118 ± 186	**7,762 ± 593** **
p-Coumaric acid	206 ± 11	**28 ± 1** ***	**52 ± 2** ***	**502 ± 1** ***	64 ± 8	**271 ± 4** ***	40 ± 6	**367 ± 27** ***
Chlorogenic acid	270 ± 7	**140 ± 2** ***	228 ± 33	**134 ± 13** ***	ND	114 ± 27	ND	ND
Quercetin derivatives	958 ± 38	**743 ± 35** **	**2,766 ± 91** ***	**4,462 ± 133** ***	552 ± 50	**3,684 ± 37** ***	461 ± 21	**1,737 ± 62** ***
	DET1 Genotypes Ripe Skin							
Phenolics (μg/g DW)	T56	2A11	TFM7	P119	MM	MM*hp2*^{j}	SM	SM*hp2*
Caffeic acid	234 ± 10	**177 ± 5** **	**173 ± 7** ***	**3,103 ± 98** ***	463 ± 94	**4,668 ± 774** **	1307 ± 38	**2,028 ± 38** ***
p-Coumaric acid	223 ± 17	**176 ± 4** *	**153 ± 23** **	217 ± 38	215 ± 21	**390 ± 11** ***	288 ± 12	**368 ± 19** **
Chlorogenic acid	346 ± 28	**1,579 ± 24** ***	**2,600 ± 63** ***	**765 ± 42** ***	509 ± 59	**749 ± 42** **	247 ± 5	**1,,010 ± 59** ***
Quercetin derivatives	547 ± 34	**1,207 ± 34** ***	**1,758 ± 50** ***	**1,921 ± 37** ***	1,298 ± 43	**4,696 ± 375** **	1267 ± 48	**2897 ± 67** ***
Naringenin-chalcone	1,900 ± 300	**706 ± 110** **	**331 ± 220** **	**775 ± 215** **	6,039 ± 491	**452 ± 441** ***	12,386 ± 1264	**4,892 ± 15,93** ***
	DET1 Genotypes Mature Green Pericarp							
Phenolics (μg/g DW)	T56	2A11	TFM7	P119	MM	MM*hp2*^{j}	SM	SM*hp2*
Caffeic acid	347 ± 25	**235 ± 18** **	**1,598 ± 104** ***	**6,588 ± 85** ***	1041 ± 80	**4,710 ± 936** *	3224 ± 68	**4,611 ± 172** ***
p-Coumaric acid	ND	ND	ND	**394 ± 1** ***	ND	**36 ± 6** ***	ND	**175 ± 13** ***
Chlorogenic acid	ND	ND	**61 ± 3** ***	**46 ± 2** ***	ND	ND	ND	ND
Quercetin derivatives	ND	**154 ± 22** ***	**810 ± 437** ***	**2,903 ± 33** ***	ND	**807 ± 78** ***	ND	**905 ± 41** ***
	DET1 Genotypes Ripe Pericarp							
Phenolics (μg/g DW)	T56	2A11	TFM7	P119	MM	MM*hp2*^{j}	SM	SM*hp2*
Caffeic acid	635 ± 10	**69 ± 2** ***	**395 ± 3** ***	**1,686 ± 37** ***	386 ± 26	**2,938 ± 40** ***	1,428 ± 29	**983 ± 17** ***
p-Coumaric acid	110 ± 0	ND	ND	**296 ± 2** ***	ND	ND	ND	ND
Chlorogenic acid	145 ± 7	**41 ± 8** ***	**333 ± 82** *	**417 ± 17** ***	148 ± 23	**391 ± 11** **	134 ± 3	**635 ± 6** ***
Quercetin derivatives	ND	ND	**341 ± 12** ***	**945 ± 43** ***	ND	1,757 ± 906	ND	970 ± 38
Naringenin-chalcone	ND	ND	ND	**50 ± 15** ***	ND	ND	ND	120 ± 90
	DET1 Genotypes							
Total anthocyanins (μg/g DW)	T56	2A11	TlFM7	P119	MM	MM*hp2*^{j}	SM	SM*hp2*
Mature green	163 ± 7	**307 ± 10** ***	**767 ± 14** ***	**1,323 ± 13** ***	239 ± 3	**697 ± 12** **	224 ± 18	**928 ± 18** ***
Red ripe	90 ± 6	**272 ± 8** ***	**212 ± 7** ***	**490 ± 21** ***	204 ± 39	245 ± 8	175 ± 9	221 ± 2

Values shown in bold are either significantly higher or significantly lower than those of the appropriate background strain. A minimum of three biological and three technical replicate measurements were performed. The data are presented as means ± SD. Student's *t* tests were used to determine significant differences between pairwise comparison between the wild-type (T56) and the transgenic varieties as well as the mutant *hp2* alleles and their respective wild-type backgrounds; $P < 0.05$, $P < 0.01$, and $P < 0.001$ are indicated by *, **, and ***, respectively. Values in bold indicate where significant differences have been found compared to the wild-type backgrounds. ND, not detected; MM, Moneymaker; SM, San Marzano.

from all three varieties (2A11, TFM7, and P119) at both the mature green and ripe fruit stages contained higher antioxidant capacities (see Supplemental Figures 1C and 1D online). The highest increases (2- and 4-fold in the mature green and ripe extracts, respectively) belonged to the P119 variety.

Cellular Phenotypes of the *DET1* Varieties

Previous studies have reported an increased plastid complement per cell as a characteristic feature of *hp* mutants (Cookson et al., 2003; Liu et al., 2004; Kolotilin et al., 2007). Visualization of cells from the *DET1* varieties supported these findings (Figure 4A, i to iv). To quantify this observation, the cell indexes were determined for all varieties using Nomarski microscopy. The cell indexes represent the total plastid area per cell versus cellular plan area, where the cellular plan area is the area of the cell's projected top view. To reduce heterogeneity among samples, different pericarp tissues and different sized cells were examined in a comparative manner with their respective controls. These data confirmed that regardless of cell size and type, the number of plastids, size of the plastids, and cell index were increased in all *DET1* varieties (Figures 4B to 4D). Collectively, the normalized

data (Figure 4D) indicated that the plastid area within TFM7 and P119 cells at the mature green stage was increased ~3-fold, whereas the increases in 2A11 were more modest (1.5-fold). To further confirm these findings, a PCR-based assay was developed to determine the plastome-to-nuclear genome ratio. The genes used in this assay were the large subunit of ribulose-1,5-bisphosphate carboxylase/oxygenase (*rbcL*) for the plastome and phytoene desaturase (*PDS*) for the nuclear genome. In the TFM7 and P119 varieties, the increase in this ratio was 2.5-fold relative to the T56 wild type (Figure 4E). Therefore, the PCR data were consistent with the physical parameters of the plastid as determined by microscopy. For comparison, the *hp2*^{J} mutant allele in the Moneymaker background was analyzed in parallel with the *DET1* varieties (see Supplemental Figure 2 online). The data sets were comparable to those of the *DET1* varieties, although the fold increases in plastid area per cell were greater in the TFM7 and P119 *DET1* varieties (e.g., 5-fold increases in TFM7 compared with 3-fold in *hp2*^{J}). These increases found in chloroplast-containing tissues were also found in chromoplast-containing tissues from ripe fruit.

Ultrastructural changes in the plastids of the *DET1* varieties were revealed by transmission electron microscopy. Using TFM7 to illustrate the findings from the *DET1* varieties, Figure 4A (ii and v) shows that the chloroplasts typically contain more membranous structures and plastoglobuli in comparison to wild-type controls. At the ripe stage of fruit development, the most striking difference was the presence of more and larger plastoglobuli (Figure 4A, iii and vi).

Metabolomic Analyses of *DET1* Downregulated Varieties

Using a combination of analytical platforms, over 120 metabolites were identified and quantified in a relative or absolute manner. Multivariate principal component analysis (PCA) was performed to calculate components and the loading contributions of each metabolite at the mature green and red-ripe stages among the *DET1* genotypes. Most of the variation (40 to 70%) arose in the first and second components. Scatterplots of components 1 and 2 showed the clearest grouping of genotypes (Figure 5). Figure 5A illustrates that at the mature green stage of fruit development, distinct separation of genotypes occurs with tight clustering of the biological replicates. The P119 genotype clusters furthest from the control (T56) in the positive sector of PC-1, and between these two are the 2A11 and TFM7 genotypes. Numerous metabolites had significant weightings, suggesting that the cluster was not due to discrete metabolites but to multiple metabolites. It was, however, observed that many of the metabolites with the highest weightings belonged to the same compound class. For example, in Figure 5A in the positive sector of the PC-1 dimension, plastid isoprenoid related compounds, such as chlorophyll and carotenoids, were found. In the opposite negative sector, amino acids and organic acids were observed.

A similar pattern was found in ripe fruit (Figure 5C) wherein the control (T56) clustered in the negative sector, with 2A11 closest to the T56 background and TFM7 closer to the P119 cluster. The isoprenoids lycopene, β-carotene, and α-tocopherol as well as phenolics such as rutin were the metabolites with the highest contributions to variation. A difference between the green and ripe fruit was the greater separation in PC-2. This was due in part to the weighting of the phytosterols (sitosterol, campesterol, and stigmasterol) and amyrins in the negative sectors of dimension PC-1 and PC-2. The initial targeted pathway analysis of these genotypes performed in this study demonstrated that many isoprenoids, phenylpropanoids, and flavonoids were elevated as a consequence of fruit-specific *DET1* downregulation. Therefore, to ascertain whether similarities and differences in metabolites between genotypes were due to intermediary metabolism, PCA was performed again but without metabolites already predetermined to be affected by *DET1* manipulation. Figure 5B is the scatterplot of PC-1 and -2 performed on metabolites from mature green tissue after removal of those pathways known to be altered, while Figure 5D is the same but with ripe fruit. It is clear in comparison to Figures 5A and 5C that the degree of clustering is less pronounced. The control (T56) and P119 genotypes again show the greatest separation predominantly along the PC-1 dimension both at green and ripe stages. At the mature green stage, the TFM7 and 2A11 genotypes cluster between T56 and P119 genotyopes, but there is separation only along the PC-2 dimension. In ripe material, 2A11 and TFM7 cluster between T56 and P119, but segregation is greatly reduced compared with Figure 5C. The metabolites contributing most significantly to the differential clustering between genotypes in the absence of isoprenoids and phenolics were amino acids and organic acids (including ascorbic acid) and the Calvin cycle intermediate sedoheptulose.

To investigate further the changes in the metabolomes of the *DET1* genotypes, metabolite changes relative to their control (T56) levels were determined and statistical analysis performed to assess the differences (see Supplemental Table 2 online). At the mature green stage of fruit development, 29, 24, and 32% of the total metabolites measured were upregulated in the 2A11, TFM7, and P119 varieties, respectively, while 8, 22, and 29% were downregulated. In the ripe fruit, 23, 24, and 42% of the metabolites were upregulated and 17, 20, and 20% downregulated in the 2A11, TFM7, and P119 varieties, respectively. The changes in metabolites followed a similar trend among all three *DET1* genotypes and in most cases correlated with the degree of *DET1* downregulation conferred by the different promoters. The changes to the metabolome were not restricted to one organelle, with metabolites synthesized in the cytosol, mitochondria, and plastid all being affected. To visually compare alterations in sectors of metabolism and interactions between metabolites, the relative changes in metabolite levels compared with their respective controls were painted onto biochemical pathway displays. Figures 6A (mature green) and 6B (ripe fruit) illustrate these changes for the P119 variety.

In mature green fruit, amino acids were reduced with the exception of Ala and Lys, and reductions were typically ~2-, 4-, and 10-fold in the 2A11, TFM7, and P119 varieties, respectively. The content of sugar phosphates and fatty acids in the green fruit was also reduced in all *DET1* genotypes compared with T56. Sugars, polyols, and organic acids were not greatly altered, although notable exceptions did occur. For example, the Calvin cycle intermediate sedoheptulose phosphate was increased significantly in the 2A11, TFM7, and P119 varieties (2-, 2-, and 10-fold, respectively). Among the organic acids, dehydroascorbic

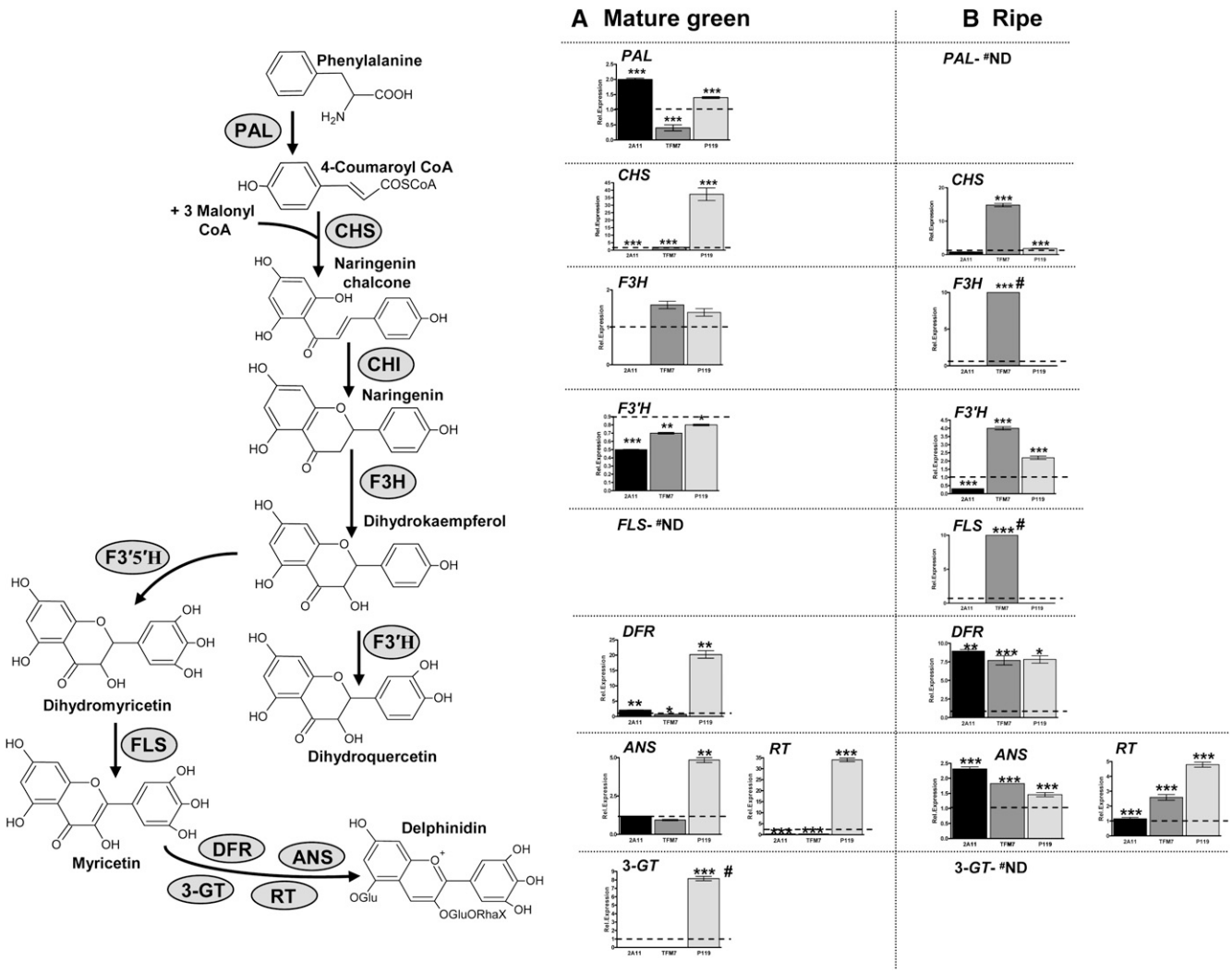

Figure 3. Changes in Gene Expression Levels of Some Key Phenylpropanoid and Flavonoid Biosynthetic Genes Resulting from *DET1* Downregulation at Both the Mature Green and Ripe Stages of Fruit Development and Ripening.

At each fruit stage, three individual fruit from three independent plants were pooled and pulverized into a homogenous powder as described in Methods. Mature green fruit represented 37 to 40 days postanthesis (dpa) and ripe 5 days postbreaker (dpb). RNA was then extracted from an aliquot of this material and three independent qRT-PCR determinations performed with gene-specific primers as detailed in Methods. Expression data were normalized to the expression of actin. Data are presented as relative levels found in the three varieties compared with the T56 wild type. Statistical determinations are provided as means ± SD value where $n = 3$ to 6. Student's t tests have been performed to illustrate statistically significant (*$P < 0.05$, **$P < 0.01$, and ***$P < 0.001$) differences from the wild-type levels. The solid black bar represents 2A11, the gray bar TFM7, and light-gray bar P119. The dashed line across each histogram indicates the relative wild-type expression level. *PAL*, phenylalanine ammonia lyase; *CHS*, chalcone synthase; *CHI,* chalcone isomerize; *F3H*, flavanone-3-hydroxylase; *F3′H*, flavonoid-3′-hydroxylase; *F3′5′H*, flavonoid-3′5′-hydroxylase; *FLS*, flavonol synthase; *DFR*, dihydroflavonol reductase; *ANS*, anthocyanidin synthase; 3-*GT*, flavonol-3-glucosyltransferase; *RT*, flavonol-3-glucoside-rhamnosyl transferase. These abbreviations for the phenolic biosynthetic enzymes have been used to annotate the pathway illustrating their position in the pathway. #ND, not detectable. The "**#**" indicates that the transcript was unique to the *DET1* variety and could not be detected in the T56 background; an arbitrary value of 10 has been used in these cases.

acid was elevated 3-, 5-, and 8-fold in the 2A11, TFM7, and P119 varieties, respectively. Further details of relative metabolite levels in mature green fruit are presented in Supplemental Table 2 and Supplemental Figures 3A and 4A online.

The amino acids present in the ripe fruit of the *DET1* varieties were at lower levels compared with those in T56 fruits, with the exception of Ala, which showed up to 2-, 2-, and 10-fold increases in the 2A11, TFM7, and P119 varieties, respectively. In the case of organic acids, phytosterols, fatty acids, sugars, polyols, phosphates, and N-containing compounds, it was difficult to deduce consistent trends among the *DET1* varieties. The most striking changes in the composition of the metabolites occurred in the P119 *DET1* variety. For example, all fatty acids were increased 3- to 5-fold in this variety, but no changes in the

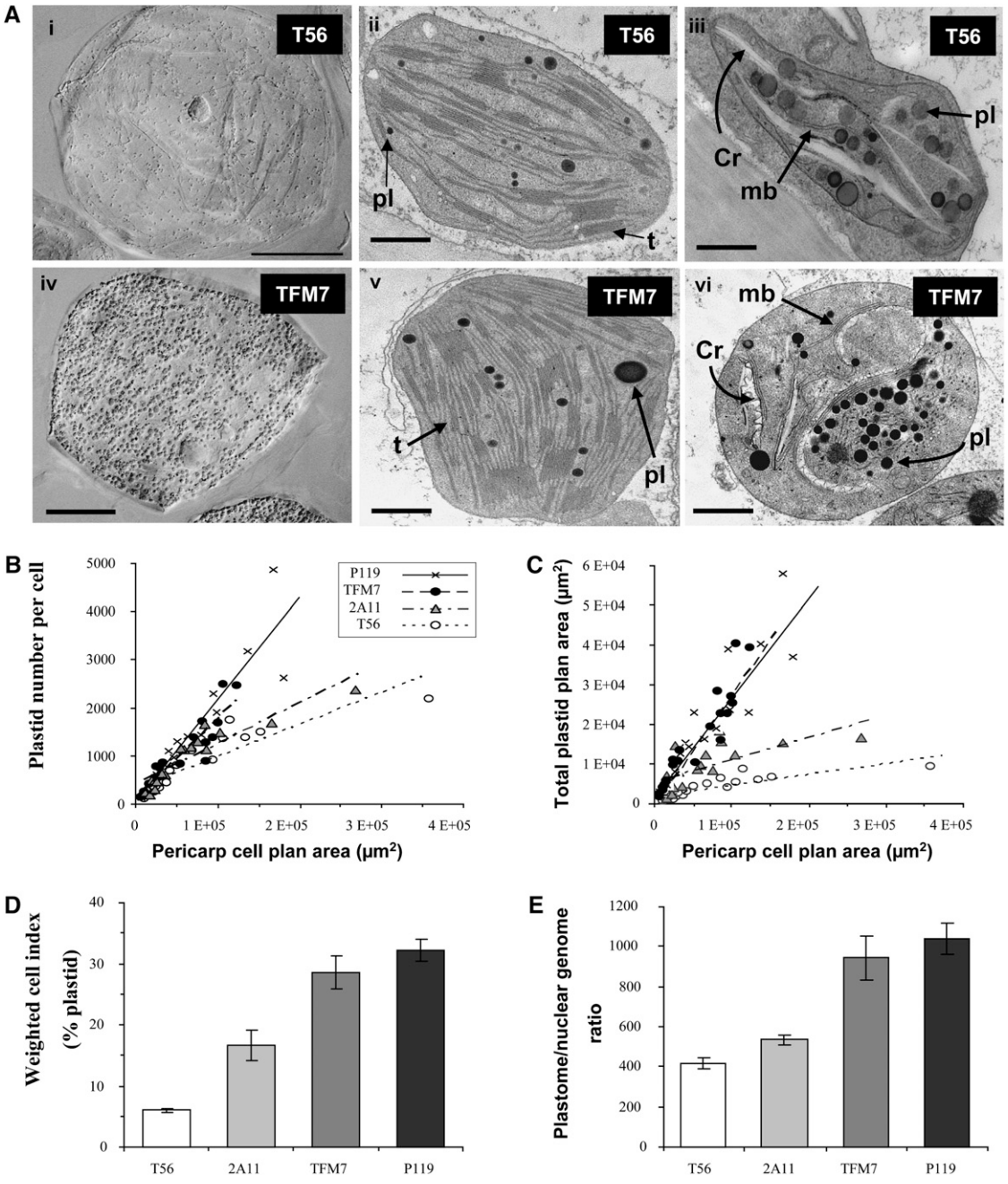

Figure 4. Changes in Plastid Parameters and Ultrastructure Resulting from *DET1* Downregulation.

(A) Panels i and iv illustrate representative control (T56) and *DET1* downregulated (TFM7) cells from mature green fruit viewed under Nomarski microscopy. The solid bars indicate 100 µm. Panels ii, iii, v, and vi are transmission electron microscopy images, with the solid bars indicating 1 µm. Panels ii and v are images of cells originating from mature green fruit from control (T56) and TFM7 downregulated varieties, respectively. Panels iii and vi are images of cells originating from ripe fruit from control (T56) and TFM7 downregulated varieties, respectively. pl, plastoglobules; t, thylakoid membranes; Cr, crystalline structures; mb, membraneous structures. Sections were prepared from three fruit from independent plants, and representative sections have been illustrated.

(B) Increases in plastid number per cell found in the *DET1* varieties as a function of cell area.

(C) Increases in total plastid area per cell regardless of cell area, found in the *DET1* varieties compared with their control, are shown.

(D) Cell index calculated from the total plastid area per cell versus the plan area (the plan area being the area of the cell's projection onto one plan) of the cell for the *DET1* downregulated varieties and their control background. These data demonstrate the increased plastid complement of the cell that results from *DET1* downregulation. Collectively, these microscopy data were compiled from three biological samples counting ~20 cells from three areas of the pericarp (60 cells) per sample; the data are represented as means ± SD.

(E) Data for a complementary genetic approach showing an increased copy number of the plastome per haploid nuclear genome in the *DET1* downregulated varieties. These data are represented as means ± SD calculated from three biological samples.

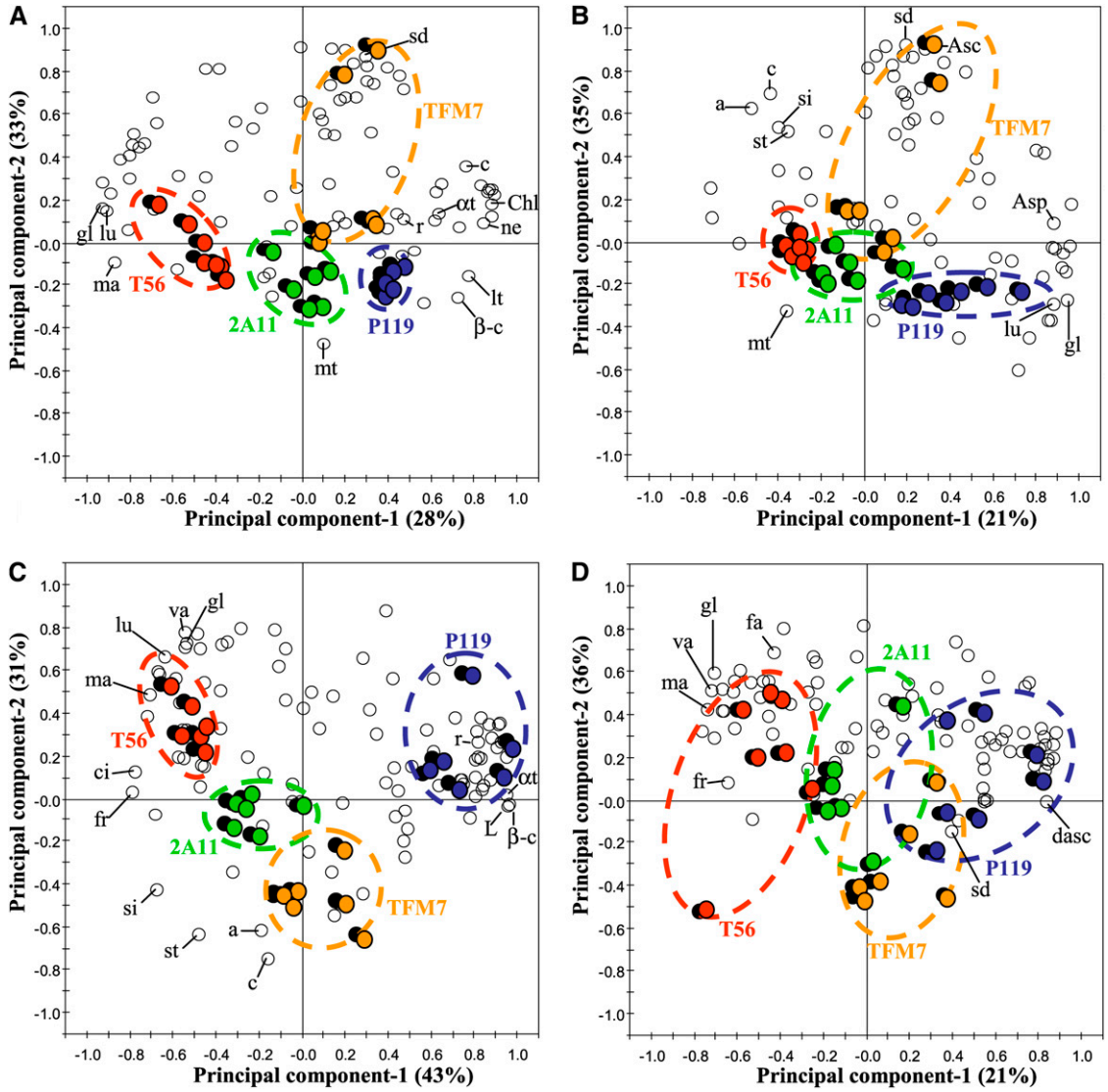

Figure 5. PCA to Assess the Variance among the Metabolite Composition of the Different *DET1* Varieties Compared with Their Background Genotype T56.

Mature green fruit samples are shown in **(A)** and **(B)**, while **(C)** and **(D)** are derived from ripe fruit. **(A)** and **(C)** were produced from data sets containing metabolite variables determined both from targeted analysis (e.g., secondary metabolites) and more untargeted analysis (e.g., primary metabolites predominantly), whereas **(B)** and **(D)** were obtained from untargeted analysis solely. Score and loadings plots were combined with solid symbols indicating genotypes and open circles representing metabolite variables. Each symbol per genotype indicates a biological replicate. Dashed ellipses have been overlaid to indicate the clustering of the specific genotypes. T56 clusters are shown as a solid red circle, P119 clusters are shown as solid blue circles, TFM7 clusters are shown as solid orange circles, and 2A11 is shown as solid green circles. The percentage provided along the axis of **(A)** to **(D)** for each component indicates the amount of variance they account for within the overall data set. Examples of key metabolites with contributions affecting the dimension of the clustering have been annotated. αt, α-tocopherol; a, amyrin; βc, β-carotene; c, campesterol; chl, chlorophyll; ci, citric acid; dasc, dehydroascorbic acid; fa, fumaric acid; fr, fructose; gl, glycine; lu, lutein; L, lycopene; r, rutin; sd, sedoheptulose phosphate; st, stigmasterol; si, sitosterol; ma, malic acid; va, valine; mt, mannitol; ne, neoxanthin.

TFM7 and 2A11 varieties were observed. All polyols analyzed were increased (2- to 8-fold) in the P119 variety, but no changes were observed in the TFM7 or 2A11 varieties. Concerning sugars, xylose, arabinose, rhamnose, glucose, gentobiose, and sedoheptulose phosphate were all increased significantly (3-fold) in the P119 variety, but only sedoheptulose phosphate showed consistent elevation in the TFM7 and 2A11 varieties. The organic acids, lactic acid, glycolate, ascorbic acid, succinic acid, 2-oxoglutarate, and dehydroascorbic acid all showed increased (2- to 9-fold) levels compared with T56, but succinic acid was the only compound to have a consistent increase among all three varieties. The levels of individual metabolites relative to their

control values in T56 ripe fruit are detailed in Supplemental Table 2 online and for P119 are displayed visually in Figure 6B. The results for the other *DET1* varieties are displayed in Supplemental Figures 3B and 4B online.

Interrogation of the metabolite data also revealed relative changes in metabolites from mature green to ripe fruit. Again the perturbations showed similar trends among the different varieties, but the effects were greater in the P119 and TFM7 varieties. The alterations were also not restricted to a specific class of metabolites or site of synthesis (see Supplemental Table 3 online). Some of the most striking increases occurred in ascorbic acid and Gln levels, which exhibited 6- and 11-fold relative increases in the P119 variety from mature green to ripe compared with the control (T56). However, sedoheptulose phosphate was an example of a metabolite that showed a relative decrease in all three varieties during ripening compared with the control.

Misregulated Transcriptional Networks Resulting from *DET1* Downregulation

Transcriptomic analysis using the TOM2 microarray was performed on the *DET1* varieties and their control (T56) using RNAs extracted from fruit at the mature green, breaker, and red-ripe stages. Validation of the array data was performed by qRT-PCR for a small subset of transcripts exhibiting a 2- to >50-fold upregulation in response to *DET1* manipulation. These data indicated a 20% coefficient of variance between the two approaches, indicating that global trends in transcript levels resulting from *DET1* downregulation can be ascertained from the array data generated.

Over all three developmental stages, a major portion of transcripts appeared to be misregulated, with upregulation of transcripts being a dominating feature during fruit development (see Supplemental Table 4 online). In the P119 and TFM7 varieties at the mature green stage, 22 and 14% of transcripts were upregulated, whereas 4 and 5% were downregulated. As predicted, the effects were most pronounced when *DET1* was under the control of the strongest promoters (P119 and TFM7); thus, further analysis was focused on these two varieties. To define the relative global effects of *DET1* downregulation on gene expression during fruit development, a set of transcripts common to all developmental stages in both the P119 and TFM7 varieties were selected on the basis of P values. This constituted 309 and 746 transcripts for P119 and TFM7 varieties, respectively (Figure 7). Boxplot and analysis of frequency distribution for expression values of all these selected transcripts revealed the overriding trend for upregulation at all development/ripening stages in both the P119 and TFM7 varieties (Figures 7A and 7B). The upregulation of transcripts was quantitatively less in the TFM7 variety, matching the comparative strengths of the two promoters. Further comparison between the P119 and TFM7 varieties also indicated other differences in the misregulation of transcripts. For example, in the P119 variety, upregulation was greatest at the mature green stage and lowest at the ripe stage, whereas the TFM7 variety possessed the greatest abundance of upregulated transcripts at the breaker stage of development. These data confirmed the global upregulation found when combining the mean fold changes for all genes over mature green, breaker, and red-ripe stages (see Supplemental Table 4 online).

The tendency of progressive reduction in gene expression during ripening in P119 was also confirmed by self-organizing maps (SOM) of the data (Figures 7C and 7D). This analysis resulted in four main trends within the P119 data sets. The first and largest group (140 transcripts) contained upregulated transcripts at the mature green stage dissipating in intensity during ripening. Group 2 (81 gene transcripts) was similar to group 1 but displayed more pronounced downregulation between mature green to breaker and breaker to ripe. Group 3 again showed the same trend as groups 1 and 2 but instead a more gradual reduction in upregulation. The last, group 4, showed patterns that were different than the negative trends found in groups 1, 2, and 3. In group 4, upregulation peaked at the breaker stage and declined thereafter. Interestingly, the latter group represented only 20% of the transcripts compared with ~80% in the other groups. SOM analysis on the TFM7 transcriptomic data set identified four groups with different trends than those found in the P119 variety. Two major groups, 1 and 4, contain roughly equal numbers of genes and show completely opposite trends. Group 1 contains 303 genes and shows a general pattern of expression that diminishes through ripening. On the other hand, group 4 (298 gene transcripts) shows highest expression at the breaker stage and a general increasing trend in expression during the ripening process. To corroborate the SOM analysis, we performed correspondence analysis (CA) of gene expression data for P119 and TFM7 (see Supplemental Figures 5A and 5B online). CA does not consider a predefined structure for the data set and hence can represent continuous variation accurately. In close conformity to the SOM results, CA also clustered gene transcripts together belonging to the same SOM group. Within each group, we were not able to find any overrepresentation of transcripts with a common biological function.

Hierarchical clustering of the array data, displayed in Figures 7E and 7F as a heat map, indicated two main clusters in P119 and three main clusters in TFM7. P119 cluster 1 formed with transcripts upregulated at the breaker stage and downregulated at the mature green stage. Cluster 2 is a heterogeneous cluster, mostly consisting of transcripts upregulated at the mature green stage and reduced through ripening. The TFM7 data sets could be differentiated into two predominant clusters. First, those transcripts upregulated at the breaker stage (cluster 1) and those upregulated at the early mature green stage (cluster 2). A cluster of transcripts upregulated from breaker to red-ripe was unique to TFM7 (cluster 3).

Transcriptional Profiling Reveals Multiple Processes and Pathways Perturbed in the *DET1* Varieties

Expression data were functionally organized into pathways and processes as detailed in the SolCyc database (http://solcyc.sgn.cornell.edu/), and changes in transcript levels in all three varieties at the mature green and red-ripe fruit stages are functionally displayed in Supplemental Figures 6A and 6B online. These data show good consistency both between varieties and stages of fruit development/ripening. For example, at the mature green developmental stage chlorophyll-, phytyl-PP biosynthesis-, and

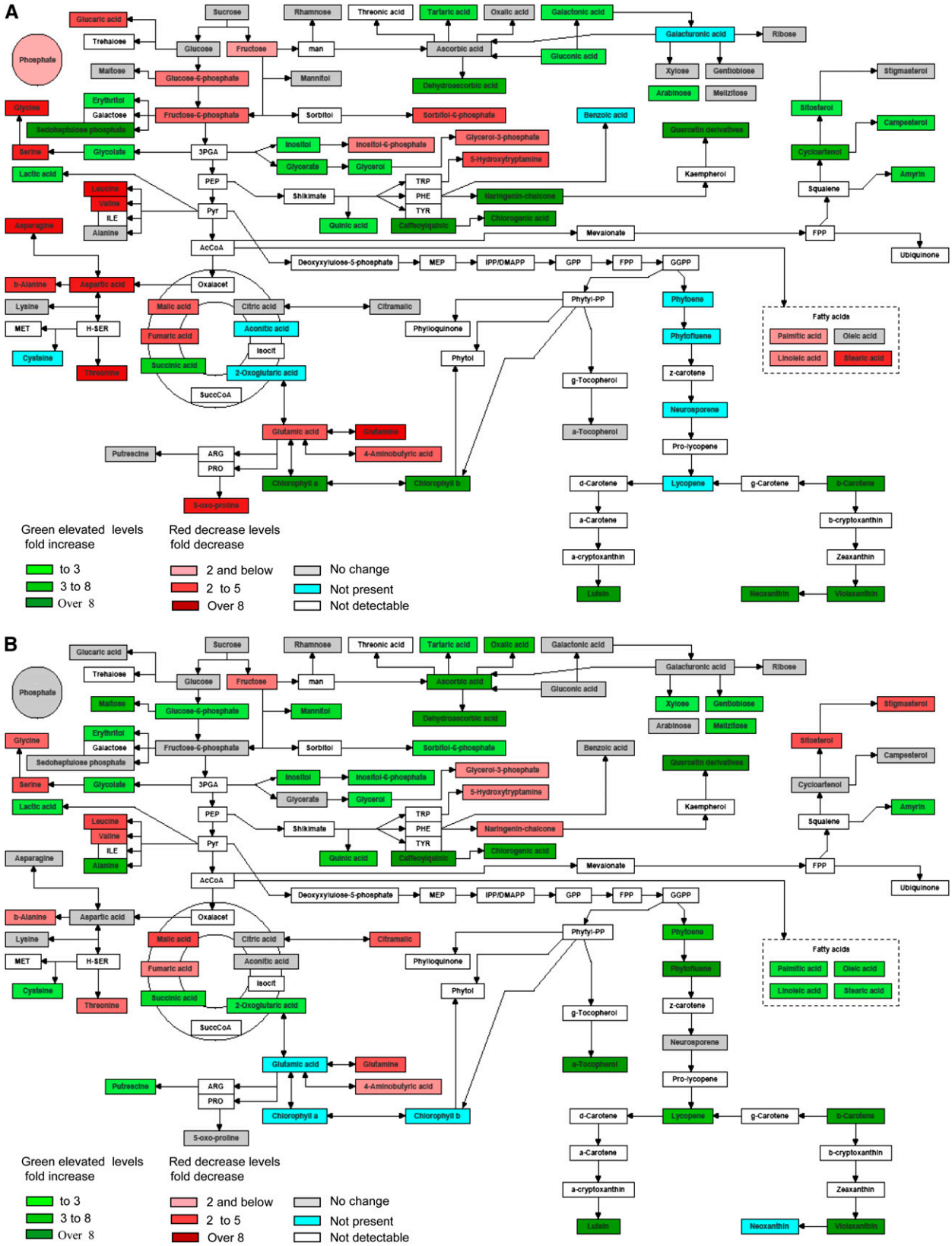

Figure 6. Metabolite Changes Occurring in Mature Green and Ripe Fruit as a Result of *DET1* Downregulation under the Control of the P119 Promoter.

photosynthesis-related transcripts encoding plastid proteins, but also transcripts for glycolytic enzymes cytosol-based glycolysis, were all upregulated in all varieties. In red-ripe fruit, the changes in the transcriptome were similar among varieties; for example, transcripts involved in aerobic respiration/tricarboxylic acid cycle cycle were upregulated ~25% and down ~13% in the P119, TFM7, and 2A11 varieties. Thus, the qualitative trends among transcripts appeared consistent. However, quantitative differences among varieties were more pronounced, and this finding is in good agreement with the targeted qRT-PCR data sets described earlier. To elucidate the hierarchy of pathways significantly affected by *DET1* downregulation, the data sets for P119 and TFM7 at each of the three developmental stages were subjected to analysis using Plant MedGen Map (Joung et al., 2009). More pathways were affected in the P119 variety in comparison to TFM7. For example, at the mature green stage, >20 pathways were significantly affected in P119 compared with only four in TFM7 (see Supplemental Table 5 online). In the P119 variety, the overriding pathways affected were chloroplast-related biochemical pathways and processes. For example, the Calvin cycle, photorespiration, and gluconeogenesis were the most affected pathways at the mature green and breaker stages and persisted into the ripe stage. The extent of upregulation of transcripts within these pathways is illustrated in Figure 8. These pathways were also predominantly affected at the breaker stage in TFM7 (see Supplemental Table 5 online). Within the TFM7 data set, transcripts involved in stress-related pathways, such as jasmonic acid biosynthesis, were also perturbed, with upregulation typically observed.

Integrative Transcript and Metabolite Analysis

To provide insight into the regulatory infrastructure associated with *DET1* downregulation, the transcript and metabolite data sets were integrated and correlation analysis performed as described in Methods. These analyses were performed with all three varieties at the mature green and ripe stages. In contrast with the predominant upregulation found with the transcript data, correlation analysis between transcripts revealed both positive and negative correlations both at the mature green (see Supplemental Figure 7 online) and ripe (see Supplemental Figure 8 online) stages. A feature of the data was the blocks of strong correlations, either positive or negative, among transcripts belonging to the same or related pathway or process. This feature was exemplified by the positive correlations observed among photosynthesis-related transcripts following *DET1* downregulation at both the mature green and ripe stages (Figures 9A and 9B, respectively). In fact, the positive correlations of multiple pathways/processes (e.g., ascorbate, chlorophyll, chorismate, and starch biosynthesis) relating to photosynthetic processes were a dominant feature of this analysis both at mature green and ripe stages (see Supplemental Figures 7 and 8 online, respectively).

Correlation analyses between metabolites in response to *DET1* downregulation are illustrated in Supplemental Figure 9 online for the mature green fruit and Supplemental Figure 10 online for the ripe fruit. A similar effect to that found with the transcripts was evident for metabolites with components of the same or related pathways having matching coresponses. Figures 9C and 9D illustrate the coresponses within the isoprenoid pathway. Interestingly, at the ripe fruit stage (Figure 9D), there was a clear differential response between plastid-derived isoprenoids and extraplastidial synthesized isoprenoids. In the mature green fruit, this distinction among different classes of isoprenoids was not observed. In contrast with the transcript-to-transcript and metabolite-to-metabolite correlations, significant agreement in correlations between transcripts and metabolites at the mature green and ripe stages were not found, as illustrated in the heat maps presented in Supplemental Figures 11A and 11B online. In this instance, both negative and positive correlations between individual transcripts and metabolites existed, but coordinated correlations between defined sectors of metabolism were not evident to the same degree either at the mature green or ripe stages (Figures 9E and 9F). The exceptions to this observation were photosynthesis- and isoprenoid-related transcripts, for which at the mature green and ripe fruit stages, positive and negative correlations predominated, respectively. To ensure that the lack of correlations between transcripts and metabolites was not solely due to developmental timing, analysis was performed between transcripts and metabolites determined at different stages in the development of fruit. These data were in agreement with the other analysis indicating reduced connectivity between transcripts and metabolites but did support the findings at mature green and ripe stages solely with regard to core processes, particularly photosynthesis-related events. For example, Supplemental Figure 11C online illustrates poor coresponses between processes occurring globally, the exception being photosynthesis, in which negative correlations between transcripts at the mature green stage and metabolites in the ripe fruit can be seen. These data are in contrast with the positive coresponses observed at the mature green stage solely, providing a logical biological confirmation to validate the data sets and their analysis.

Figure 6. (continued).

The metabolomic data are displayed quantitatively over schematic representations of biochemical pathways produced with BioSynLab software (www.biosynlab.com). False color scale is used to display the quantity of each metabolite in P119 relative to that in T56. Pale green indicates a significant threefold increase, a 3- to 8-fold increase is green, and >8-fold is dark green. Gray indicates no significant change, whereas blue indicates that the metabolite was not detected in the samples. White indicates that the compound cannot be detected using the analytical platforms available. Red coloration has been used to represent decreased metabolite levels; dark red is below 8-fold, red is below 2- to 5-fold, and pale red is below 2-fold. Aco, aconitic acid; L-Asc, ascorbic acid; citramal, citramalic acid; Cit, citric acid; dehydroasc, dehydroascorbic acid; Fum, fumaric acid; Mal, malic acid; 2-oxoglut, 2-oxoglutaric acid; Succ, succinic acid; Thre, threonic acid; 5HT, 5-hydroxytryptamine; 5-OxoPRO, 5-oxo-proline; Arab, arabinose; DXP, deoxyxylulose-5-phosphate; F6P, fructose-6-phosphate; G6P, glucose-6-phosphate; 3-CaQuinic, 3-caffeoylquinic acid; CGA, chlorogenic acid; FPP, farnesyl diphosphate; GPP, geranyl diphosphate.

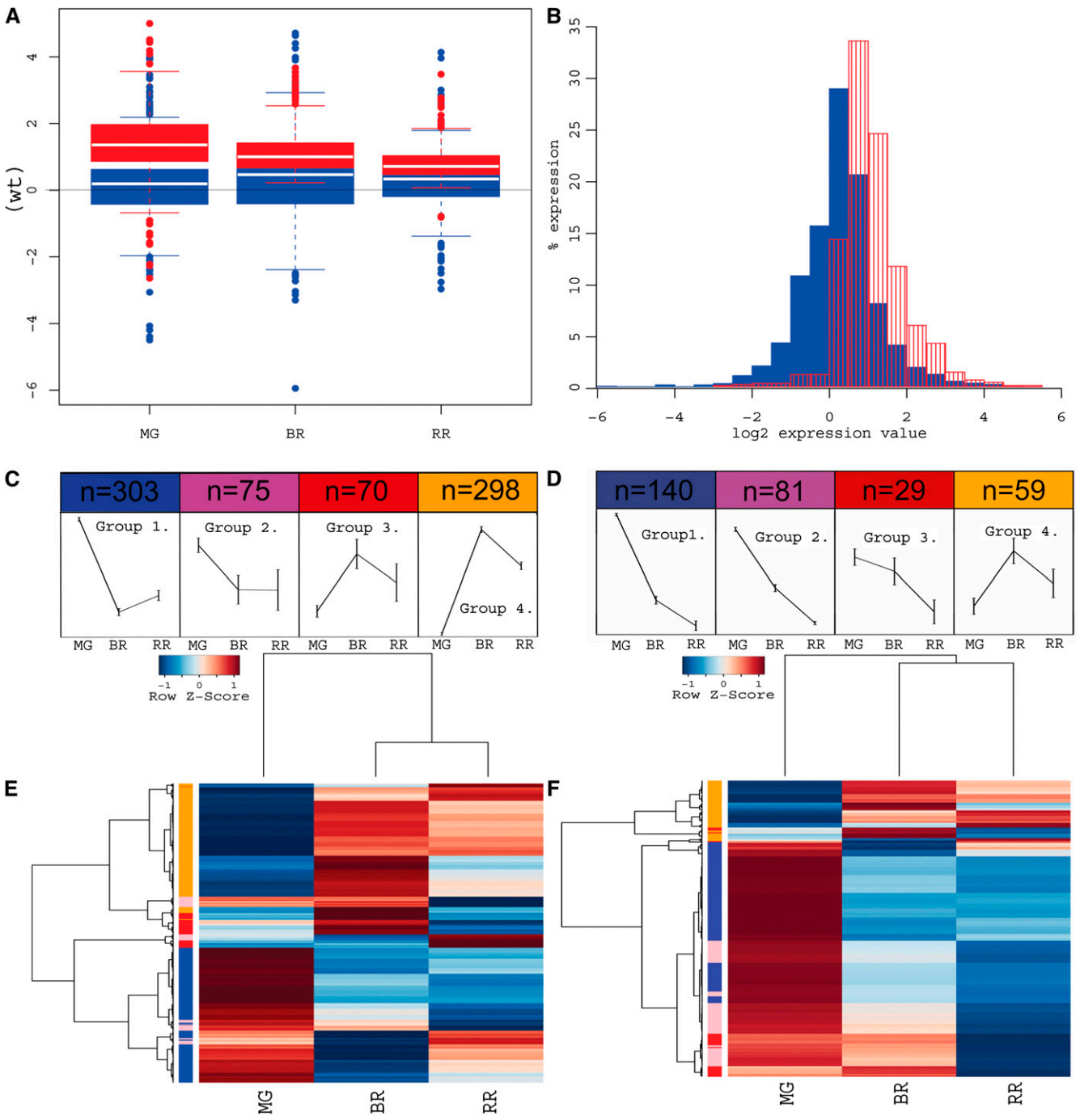

Figure 7. Transcriptional Misregulation Resulting from *DET1* Downregulation.

The stages of fruit development at which the analysis were performed are indicated by MG (mature green), BR (breaker), and RR (red ripe).

(A) Boxplots for log2 ratio (transgenic versus T56) of microarray expression data. P119 is shown in red and TFM7 in blue. Boxes show center quartiles (middle 50% of the data, whiskers extend to the most extreme data points that are no more than 1.5 times the interquartile range). The outliers are shown as filled circles.

(B) Frequency distribution of expression values for P119 (red) and TFM7 (blue) across all developmental and ripening stages. The *x* axis represents log2 expression ratio of the *DET1* variety versus T56 (control), indicating the relative changes in transcripts occurring within the data sets. The *y* axis shows the percentage of transcripts with a given relative expression value. An overwhelming proportion of expression values are above the T56 control level for P119, but TFM7 shows significant downregulation.

(C) and **(D)** SOMs for TFM7 **(C)** and P119 **(D)**. In each partition, the pattern reflects a general trend of expression gradient of the group across three

DISCUSSION

Biotechnological Implications of the *DET1* Downregulated Fruit Chemotype

The targeted metabolite profiling approach used here has determined the diversity and content of the health-related phytochemicals present in *DET1* downregulated fruit. The levels of the individual antioxidants are in most cases comparable to those achieved by other genetic engineering approaches (Verhoeyen et al., 2002; Apel and Bock, 2009; Fraser et al., 2009). However, the unique feature of the *DET1* chemotype is the simultaneous enhancement of multiple antioxidants that originate from diverse biochemical pathways and function in both the polar and nonpolar cellular environments. To date, the only report demonstrating simultaneous increases in multiple nutritional components is the xenogenic pathway engineering of maize (*Zea mays*; Naqvi et al., 2009), in which multiple gene products sourced from bacteria were used. However, such an approach has important regulatory restrictions and is less acceptable to the consumer. In comparison, the *DET1* chemotype has been created using a *cis*-genic approach with a single endogenous plant gene product.

The data presented here and reported previously (Davuluri et al., 2005) also highlight that only small reductions at specific developmental stages are required (or tolerated) to achieve significant enhancement of these beneficial phytochemicals. This suggests that exacerbation of *DET1* downregulation would have a detrimental effect on fruit viability in a manner akin to the constitutive expression previously reported (Davuluri et al., 2004) and that natural alleles of *DET1* are weak in their effectiveness, as stronger mutations would be lethal to the plant. In fact, the *DET1* GM varieties (e.g., 2A11, TFM7, and P119) do exhibit a higher fold increase in antioxidant compounds compared with their natural (non-GM) counterparts (e.g., the *hp* mutant alleles), without the loss of plant vigor. Collectively, these data would therefore question TILLING (Triques et al., 2007) or molecular-assisted selection as effective approaches to deliver high nutrient fruit because modulation of fruit-specific *DET1* expression is unlikely to be achieved by these approaches. Thus, the GM approach adopted (Davuluri et al., 2005) represents the most plausible strategy if optimal levels of the antioxidants in question are the predominant criteria. Beyond tomato, the potential lethality of *DET1* downregulation in vegetative tissues also questions its utility in increasing multiple antioxidants in leafy vegetable crops.

The antioxidant assays performed demonstrate that the increases in metabolites could be translated to increased antioxidant capacity of the fruit both in the polar and nonpolar phases. The increases in antioxidant capacities were either comparable or, if polar and nonpolar activities were combined, greater than the polar activities reported as a result of high flavonoid or hyperanthocyanidin production (Butelli et al., 2008; Luo et al., 2008). Presumably, this suggests that either other polar antioxidants are elevated in the *DET1* downregulated varieties or that saturation of antioxidant activity can occur at high concentrations in endogenous extracts.

The Effect of *DET1* Downregulation on the Global Regulatory Infrastructure

The *DET1* gene product is predominantly involved in the transduction of an environmental signal, which initiates an appropriate adaptation of processes and metabolisms to the plants' surroundings, in this case light (Schäfer and Bowler, 2002). The effects of *DET1* are implemented through its ability to modulate the stability of transcription factors, some of which have multiple potential gene targets (Osterlund et al., 2000; He et al., 2007). Moreover, the DET1 protein has the capacity to bind histone H2B in vivo (Benvenuto et al., 2002) and may therefore alter the chromatin context of DNA, potentially exposing the DNA around target genes to facilitate transcription. Therefore, it is not surprising that the effects of perturbation of *DET1* are widespread throughout metabolism as witnessed from the metabolomic and transcriptomic analyses herein performed. It can be envisaged that binding of DET1 or of other downstream transcription factors onto chromatin/DNA could result in (1) transcription of global regulators and or transcription factors, (2) mediation via signal transduction proteins, (3) release of attenuating transcription factors or coordinated transcription of genes, and (4) direct action on genes encoding biosynthetic pathway components. In addition, the balance of the small molecules generated by these changes may in turn further affect transcription of related genes.

The predominance of upregulated gene transcripts revealed by transcript analysis suggests that *DET1* is a negative regulator. The transcription of global regulators associated with ripening (e.g., *nor*, *rin*, or *CNR*; Giovannoni, 2004) as well as those transcription factors represented on the array were not perturbed by *DET1* downregulation, suggesting that within the limits of the TOM2 array the chemotype of *DET1* downregulation was not initiated by a limited number of cardinal transcription factors. Instead, the correlation analysis of transcripts revealed blocks of transcripts responding in a coordinated manner to *DET1* downregulation. These blocks consisted of genes with related functionality. In addition, a strong degree of connectivity was observed among these pathway and process components. Thus, coordinated transcriptional activation would appear to

Figure 7. (continued).

developmental stages with vertical bars showing the variance in the group at each stage. A gene is assigned to a single partition with similar groups placed in nearby partitions.

(E) and **(F)** Heat maps of the gene expression data for TFM7 **(E)** and P119 **(F)**. Each horizontal line represents the gene expression across the three developmental stages. For each gene, log2 expression ratios of *DET1* variety versus T56 are normalized across the three stages. Red indicates upregulation and blue downregulation with respect to the T56 background. The z-scores have been used to indicate the deviation from normal distribution (the distribution standard derivation) and calculated from the variable's value minus the population's mean divided by the SD of the population. The vertical color bars next to gene trees indicate genes belonging to SOM classes in **(C)** and **(D)**.

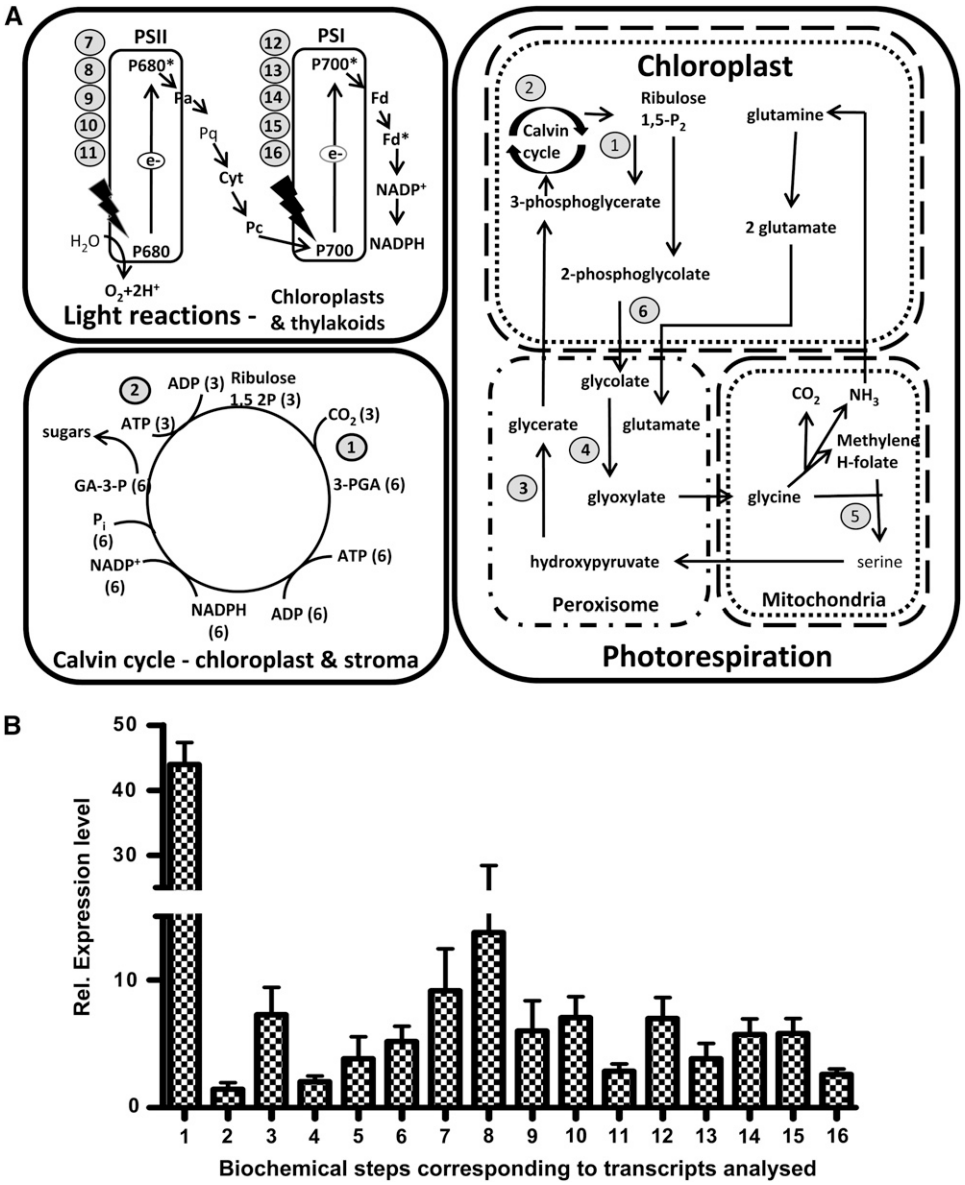

Figure 8. The Effect of *DET1* Downregulation on Photorespiration-Related Gene Expression Levels in P119 Mature Green Fruit.

(A) Pathways and processes involved in photorespiration; steps in the pathways where transcripts have been measured are numbered.
(B) Changes in gene expression levels relative to levels determined in control (T56 background) samples. Data from microarray analysis have been used; the experimental design of these experiments is provided in Methods. The data are expressed as means ± SD. Transcripts are labeled as follows, 1, ribulose-1,5-bisphosphate carboxylase small chain 3b; 2, glycolate oxidase; 3, hydroxypyruvate reductase; 4, glycine hydroxymethyl transferase; 5, transketolase; 6, phosphoglycolate phosphatase; 7, photosystem II protein 16; 8, photosystem II 22-kD protein; 9, photosystem II 5-kD protein; 10, photosystem II psbY; 11, photosystem II reaction center; 12, photosystem I subunit II; 13, photosystem I subunit III; 14, photosystem I subunit VI; 15, photosystem I subunit X; 16, photosystem I subunit psaN. Pa, pheophytin; Pq, plastoquinone; Cyt, cytochrome *bf* complex; Pc, plastocyanin; Fd, ferrodoxin; 3-PGA, 3-phosphoglycerate; GA-3-P, glyceraldehyde-3-phosphate. Stoichiometries of Calvin cycle components shown in parentheses.

play an important role in the implementation of the phenotypes associated with *DET1* downregulation. These findings are in agreement with the genome-wide coexpression networks elucidated from *Arabidopsis thaliana* data sets (Wei et al., 2006). In these studies, the strongest transcriptional coordination exists among and between core pathways such as those related to photosynthesis (e.g., Calvin cycle and photorespiration). The transcriptional coexpression analyses performed with the *DET1* data sets corroborate these findings. Likewise, correlation analysis between metabolites of related pathways and among metabolites of the same pathway exhibited significant coordination in responses to *DET1* downregulation. This finding was particularly

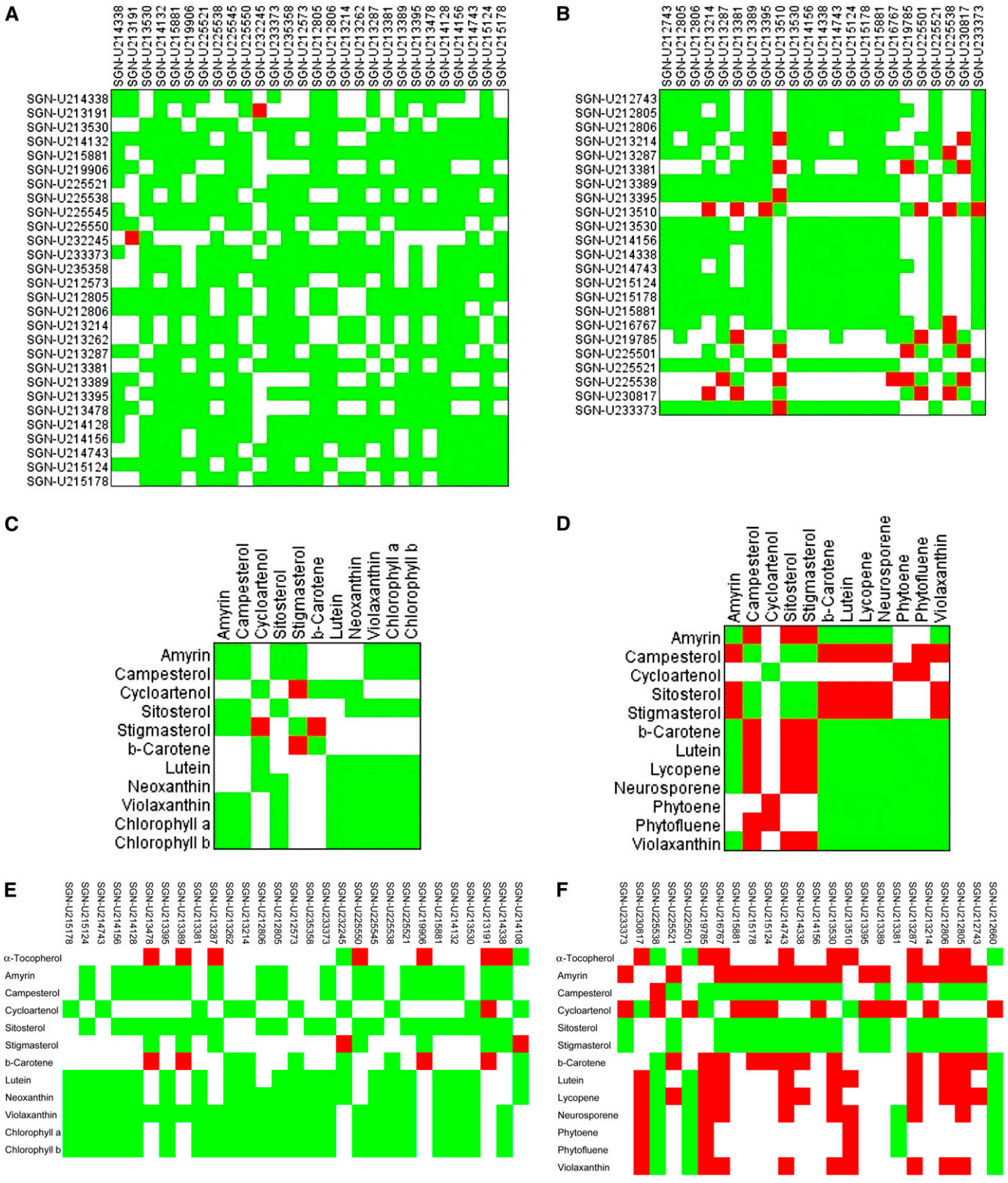

Figure 9. Selected Heat Maps Showing Intrapathway/Process Correlations between Photosynthesis-Related Transcripts and Isoprenoid Metabolites.

(A) and **(B)** Coresponses between photosynthesis-related transcripts in mature green and ripe fruit, respectively.

(C) and **(D)** Coresponses between isoprenoid metabolites in mature green and ripe fruit, respectively.

(E) and **(F)** Coresponses between isoprenoid metabolites and photosynthesis-related transcripts in mature green and ripe fruit, respectively. A false color scale is used to indicate positive (green) and negative (red) correlations. Stringent cutoff coefficient values of either 0.8 or −0.8 have been used with a significance of $P < 0.05$. Pearson correlation coefficients (r) were calculated using data sets for all the *DET1* genotypes, with triplicate biological replication per genotype. Calculations were performed using BioSynLab software (www.Biosynlab.com)

evident for metabolites involved in core processes. Photosynthesis-related transcripts also exhibited positive coresponses with isoprenoid metabolites at the mature green developmental stage. These data support the essential role of isoprenoids like chlorophyll and xanthophylls in photosynthesis as well as phytosterols in cell elongation and development. A complementary set of coresponses were observed at the ripe stage in which photosynthesis-related transcripts possessed a negative correlation with isoprenoids. Such data reflect the changing metabolic and physiological requirements of fruit during ripening with a shutdown of photosynthesis, cell elongation, and accumulation of chromoplast-associated pigments with no photosynthetic functionality (Gillaspy et al., 1993). Despite the correlations observed between photosynthesis-related transcripts and isoprenoids, a global lack of correlation between transcripts and metabolites is evident. These findings do not support the traditional view that transcriptional regulation drives subsequent translation (protein levels), enzyme activity, and metabolite content. Instead, it would appear that in the case of *DET1*, posttranscriptional regulation plays a key role. The lack of correlations between metabolites and transcripts also suggests that metabolites are not playing a key role in modulating transcription either. Perhaps the regulatory effects of small molecules in this case occur at the level of translation. More data collection at the different regulatory levels will possibly elucidate such mechanisms. These data also suggest that the isolated use of transcriptomic data for the elucidation of regulatory networks is restrictive.

The Transcript and Metabolite Changes Associated with *DET1* Downregulation Reflect Its Role in Mediating Responses to Light

The effect of light on plant development has been studied extensively in many species (Terzaghi and Cashmore, 1995). A number of pathways and processes are known to be transcriptionally activated by light (Ghassemian et al., 2006). These include photosynthesis, the Calvin cycle, chlorophyll, and flavonoid biosynthesis, as well as a number of stress-related processes (Cominelli et al., 2008). In the *DET1* downregulated fruit, all these processes/pathways are upregulated and show a positive inter- and intrapathway correlation. This supports previous transcript analysis performed on *hp2* alleles (Kolotilin et al., 2007). Therefore, in effect, it would appear that a pseudostate of light hyperresponsiveness has been created in developing tomato fruit via *DET1* downregulation, mimicking the molecular responses to high light conditions, as already observed for several *Arabidopsis* photomorphogenic mutants (including *det1-1*) (Ma et al., 2003). This in turn has resulted in the coordinated transcription of light-related biochemical pathways and processes, in particular those associated with photosynthesis. This shift in or enhancement of existing metabolic events is perfectly plausible from a biochemical viewpoint because the enhanced perception of light could signal a shift toward increasing light use by the photosynthetic apparatus. The subsequent products of the photosynthetic light reactions are ATP and $NADPH_2$, which sustain the Calvin cycle, facilitating the fixation of CO_2 into sugar. The Calvin cycle in turn is a component of photorespiration. These primary events mediated by *DET1* also provide an explanation as to why the *DET1* downregulated phenotype arises primarily in developing chloroplast-containing tissues and why the timing of promoter control is crucial. For *DET1* to mediate its metabolic effects, the cell type should be primed for core metabolic events (e.g., photosynthesis). Presumably this is also why such large differences in metabolite and transcript profiles are found in spite of only subtle differences in the developmental profiles of *DET1* downregulation under the control of the P119 and TFM7 promoters. It is therefore not so surprising that ripening-specific downregulation of *DET1* has no phenotypic effect (Davuluri et al., 2005) because these specialized chromoplast-containing tissues are not designed for vegetative core metabolic events.

With the dampening effects of *DET1* attenuated through downregulation, it is expected that a number of stress-related transcripts would also be upregulated, as the plant effectively perceives greater light incidence, creating the potential for high light stress. For example, the formation of phenolics and ascorbate along with transcriptional changes in lipoxygenase and jasmonate biosynthesis pathways have all been associated with light-related stress responses (Youssef et al., 2009).

Photomorphogenesis has been intensively studied (Ma et al., 2001; Foo et al., 2006; Ghassemian et al., 2006; Lopez-Juez et al., 2008) and specifically the role of *DET1* in light adaptation (Chory et al., 1989; Schroeder et al., 2002). The transcriptional and metabolite changes determined in the mature green fruit of the *DET1* varieties were in general agreement with these studies. Therefore, in developing tomato fruit, the changes occurring are likely in part to reflect the function of *DET1* in chloroplast-containing tissues and its consequences.

How Does the Perturbation of *DET1* Lead to Increased Antioxidant Content in Tomato Fruit?

Integrative analysis of transcripts and metabolites has highlighted core intermediary processes and stress responses as the progenitors of increased antioxidants in fruit. Interestingly, the antioxidants in question are classical secondary metabolites in tomato. Therefore, (1) how does *DET1*'s impact on core processes affect secondary metabolites? And (2) why do its effects persist after downregulation ceases?

It would appear that the flavonoids and anthocyanidin pathways are transcriptionally regulated at influential steps in the pathway (e.g., *CHS* and *DFR* in the case of flavonoid and anthocyanidin, respectively). In plant tissues, these compounds have a protective role against the damaging effects of high light incidence. Their upregulation has been demonstrated previously in response to light and other stress conditions (Cominelli et al., 2008; Lopez-Juez et al., 2008) as well as in *Arabidopsis det1* mutants. In the particular case of *CHS*, transcriptional derepression could be shown using a CHS:GUS transcriptional fusion in a *det1-1* background (Chory and Peto, 1990). Therefore, considering that the downregulation of *DET1* has created a pseudostate of light hyperresponsiveness and abiotic stresses, it is logical that the elevation of flavonoids and anthocycidins would arise. Whether *DET1* has a direct or indirect effect on transcriptional upregulation of these pathways awaits elucidation, although the altered transcript levels of several MYB and bHLH transcription

factors, which are well-established players in the regulation of flavonoid pathways (Allan et al., 2008), suggest that an indirect effect is likely. Altogether, close to 30 putative transcription factors were misregulated in P119 fruits, further suggesting an indirect effect of DET1 on transcription. It was also noted that the gene encoding *GIGANTEA*, a nuclear protein associated with light signaling in *Arabidopsis* (Huq et al., 2000), is downregulated in the TFM7 and P119 varieties.

In contrast with phenolic biosynthetic pathways, none of the transcripts encoding carotenoid and general isoprenoid biosynthetic components are upregulated in the *DET1* varieties, suggesting that posttranscriptional regulation is operational. Notwithstanding, the upregulation of transcripts encoding tocopherol biosynthetic steps does suggest that transcriptional regulation is involved in this related branch of the pathway. The abundance of transcripts encoding plastid-related proteins and the confirmatory determination of an increased plastid compartment per cell are the likely explanation for increased carotenoid formation in these varieties. Presumably the increase in plastid area per cell creates a collective increase in biosynthetic capacity. The reason for an increased plastid cellular compartment is unlikely to be a specific effect, but rather the coordinated effects of *DET1* on plastid-related events and the need for increased plastid biogenesis per se. For example, the expression of neither transcription factors involved in plastid biogenesis (e.g., *GLK*-like; Fitter et al., 2002; Yasumura et al., 2005) nor structural proteins involved in plastid biogenesis (e.g., ribosomal proteins) or plastid division (*FtsZ* and *MinD*) (Aldridge et al., 2005) were affected substantially (< or >1.5-fold) in the *DET1* varieties. These data contradict findings with the natural alleles and may reflect the constitutive effects of the natural alleles on events associated with aspects of vegetative development. The effects on core metabolic processes are, however, common to the *DET1* varieties, *hp* alleles (Kolotilin et al., 2007), and photomorphogenesis studies in *Arabidopsis* (Ghassemian et al., 2006). Collectively, these data could suggest that it is the initiation of core metabolic processes that drive subsequent plastid biogenesis to provide a defined cell compartment for these processes. The division or premature differentiation (Fraser et al., 2007; Maass et al., 2009) of plastids does not appear to be dramatically affected by *DET1* modulation, as increased plastid numbers with a reduced area were not evident and detectable levels of chromoplast-specific carotenes were not found.

Another explanation for global increases in antioxidants could be that increased metabolic activity within the cell leads to the generation of reactive oxygen species (ROS) or nitrogen species. To dissipate the detrimental effects of these molecules, the synthesis of protective antioxidants, such as carotenoids, tocopherols, phenolics, and ascorbate, would be advantageous (Foyer and Noctor, 2005). Therefore, the increases in antioxidants observed could simply result from the cells' natural protective mechanisms against free radical imbalances. The increases in some of the antioxidants, such as carotenoids, could also have secondary benefits in maintaining levels of other related compounds. For example, the increased pool of carotenoids could well provide protection against chlorophyll damage and contribute to the persistence and increased levels of chlorophyll. Elevation of ROS can also lead to the activation of stress responses (Foyer and Noctor, 2005). Several of the stress-related pathways misregulated by *DET1* have been associated with ROS generation (e.g., jasmonate formation and lipoxygenase activation) (Vanderauwera et al., 2005). Interestingly, the activity of lipoxygenases initiate the formation of jasmonates (Wasternack, 2006), and the latter have also been implicated in altering chloroplast parameters within the cell as well as the levels of anthocyanidins and other antioxidants (Jung, 2004; Sasaki-Sekimoto et al., 2005). More recently, altered levels of the stress-related phytohormone abscisic acid in the *hp*3 mutant, affected in zeaxanthin epoxidase (*Zep*), has been shown to alter the total chloroplast area per cell, which presumably leads to the plant's elevated carotenoid content (Galpaz et al., 2008). It would be informative to ascertain in this case if similar perturbations in metabolism arise and, if so, to correlate them with those observed with *DET1* downregulation.

To use the effect of *DET1* to generate antioxidants, this study and previous studies (Davuluri et al., 2005) indicate that downregulation in developing fruit tissues with active chloroplast proliferation is the key. However, the effects remain or are exacerbated in ripe fruit after *DET1* expression has ceased. Presumably this arises from the metabolic changes established at the earlier developmental stages. It is feasible that through increasing core metabolic events in developing fruit, a greater pool of primary metabolites for use in secondary metabolic pathways could exist. In addition, more reductant may be generated to drive associated secondary pathways. For example, glyceraldehdye-3-phosphate is a component of the Calvin cycle and a precursor of the plastidial isoprenoid biosynthetic pathway. Our metabolite profiling illustrated the large increases in sedoheptulose phosphate occurring in this pathway. Throughout isoprenoid biosynthesis there are also numerous steps that use reductant in their catalysis. It is also feasible that the increased plastid area improves sequestration of metabolic end products eliminating inhibitory feedback of the biosynthetic pathway. In support of this, the misregulation of transcripts did reveal that certain core intermediary metabolic processes persisted into ripening fruit in comparison with their controls (e.g., photosynthesis and the Calvin cycle). Such an extension of their developmental effectiveness could also play a role in delivering more usable precursors for metabolism in the ripening fruit.

In conclusion, the integrative transcript and metabolite approaches used have proven invaluable in providing insight into the changes in the cell's regulatory infrastructure and reprogramming of metabolism associated with *DET1* downregulation. The sequence of events leading to the simultaneous enhancement of multiple biosynthetically unrelated antioxidants can now be verified in a systematic manner using conventional biochemical approaches. These approaches will permit the elucidation of further targets for the optimization of nutritional antioxidant levels in plants.

METHODS

Generation and Preparation of Plant Material

Tomato (*Solanum lycopersicum*) varieties used included the T56 industrial processing genotype as the background for the P119, TFM7, and 2A11 *DET1* downregulated genotypes (Davuluri et al., 2005). The *hp2*^{j}

mutant allele in the Moneymaker variety background and the *hp*2 mutant in the San Marzano background were also used. Details of the phenotypes and recommendations for growth can be found on the Tomato Genetic Resource Centre (TGRC) at www.tgrc.ucdavis.edu. Seeds for these two *hp* mutant varieties and their respective backgrounds were also obtained from TGRC. Tomato plants were glasshouse grown from seed under supplementary lighting. Routinely, six plants per genotype were grown in a randomized manner concurrently with their respective backgrounds. Figure 1 illustrates the designations used to defined the stages of fruit development and ripening used in this study. The breaker stage representing the initial onset of ripening was taken as the first sign of color and ripe fruit as 7 d postbreaker.

Molecular Analysis

Measurement of Gene Expression by Real-Time qRT-PCR

Three fruit from independent plants of the same genotype were harvested at a similar time in the day. Tissue was prepared by cutting the fruit in half, the seeds and jelly removed, and then frozen immediately in liquid nitrogen. These fruit samples were pooled and broken down in a mortar and pestle. Complete homogenization into a powder was then performed using a freezer mill (CertiPrep/6750 apparatus; SPEX). For quantitative real-time RT-PCR determinations, RNA was extracted from 100 mg of milled tissue, while RNAs for microarray analysis were extracted from the same material but in large quantities as described in subsequent sections. The RNeasy reagents and protocol (Qiagen), including on-column DNaseI digestion, were used. The QuantiTect SYBR Green one-step real-time RT-PCR kit (Qiagen) was used to determine gene expression levels. Determinations used 25 ng of RNA, and primers were added to provide a final concentration of 0.3 μM in a final reaction volume of 20 μL. Reactions were performed on a Rotor-Gene 3000 thermocycler (Corbett Research). Thermocycling conditions were 30 min at 50°C for reverse transcription, 15 min at 95°C, followed by 30 to 40 cycles of 15 s at 94°C, 30 s at 56°C, and 30 s at 72°C. Sequencing of PCR products and melt curve analysis verified their specificity. For quantification, calibration curves were run simultaneously with experimental samples, and Ct calculations were performed by Rotor-Gene software (Corbett Research). The actin gene served as reference for normalization. Primers for real-time qRT-PCR were designed using Primer3 software (http://biotools.umassmed.edu/bioapps/primer3_www.cgi). The primers used for the PCR amplification are provided in Supplemental Table 6 online.

Determination of Plastome: Genome Ratios by Real-Time PCR

The gene encoding the large subunit of ribulose-1,5-bis-phosphate carboxylase/oxygenase (*rbcL*) was used as a plastome marker, while the *PDS* gene was used as the nuclear genome marker. A PCR-based assay was developed to determine the ratios between the two and thus provide a rapid quantitative indication of changes in the plastid content of the cell. Typically, three fruit from independent plants of the same genotype were sampled as described in the previous section. DNA was extracted from 100 mg of powdered sample using the DNeasy reagents and protocol (Qiagen). The QuantiTect SYBR Green PCR kit (Qiagen) was used to determine the number of copies of each gene per 20 ng of DNA in each sample. Primers were added to a final concentration of 0.3 μM in a reaction volume of 20 μL. Reactions were performed on a Rotor-Gene 3000 thermocycler (Qiagen). Thermocycling conditions were 95°C for 15 min followed by 40 cycles of 15 s at 94°C, 30 s at 50°C, and 15 s at 72°C. Sequencing of PCR products plus melt curve analysis verified the reactions' specificity. For quantification, calibration curves were run simultaneously with experimental samples, and actin was used as a reference gene for normalization of the data. The primers used for the PCR amplification are provided in Supplemental Table 6 online.

Microarray Analysis

Transcriptional profiling was performed using the TOM2 long oligonucleotide array platform consisting of 12,000 unigene sequences (www.ted.bti.cornell.edu). Biological replication for transcriptome analysis was created using a minimum population of six plants per genotype further sorted into pairs of plants. From each plant within a given pair, three fruit were collected and pooled to generate a biological replicate of six pooled fruit. A minimum of three such pools were generated for each genotype from fruit harvested at the mature green, breaker, and ripe stages. Pericarp tissue (including the peel) was prepared from fruit using a freezer mill as described earlier. The expression profiling experiments were designed for the comparison of each *DET1* transgenic genotype at each fruit stage to the respective T56 fruit stage as the control. Data were generated from a minimum of three biological replicates, each with a duplicate dye swap and creating a total of between six and eight hybridizations.

Protocols used for RNA extraction, cDNA synthesis and labeling, microarray hybridizations, and scanning are all available online at the Tomato Functional Genomics Database website (www.ted.bti.cornell.edu). In brief, total RNA extraction was performed from frozen powdered pericarp tissue (~5.0 g) as described by Griffiths et al. (1999). cDNA synthesis and labeling with Cy3 and Cy5 (Cy Dye Postlabeling Reactive Dye Pack; GE Amersham) was performed indirectly using the amino-ally method (Invitrogen SuperScript indirect cDNA labeling kit) according to Alba et al. (2004). Hybridizations of Cy-labeled cDNA targets to the TOM2 oligoarray were performed at 42°C for 14 to 16 h in the dark. Following hybridization, slides were washed twice in 1× SSC containing 0.2% (w/v) SDS at 43°C for 3 min and then washed in 0.1× SSC containing 0.2% (w/v) SDS at room temperature for 3 min. Slides were finally dipped in 0.1× SSC containing no SDS to remove excess SDS before washing three more times for 3 min each in 0.1× SSC solution. Scanning of arrays was performed on a two-channel confocal microarray scanner (ScanArray5000; GSI Lumonics) with ScanArray software v3.1 (Packard Biochip Technologies). Scans were performed at a resolution of 10 μm. Excitation/emission settings were 543/570 nm and 633/670 nm for the Cy3 and 5 fluors, respectively. Numerical images were generated from the microarray images using ImaGene software (version 5.5; BioDiscovery). Those spots with low intensities (i.e., less than the local background) and of poor quality were flagged by the software and not included in subsequent statistical analysis. Normalization used the print-tip strategy and was applied to ratio values for each array using the marray package in Bioconductor (Yang et al., 2002). Differentially expressed genes were identified using patterns from gene expression (Grant et al., 2005). Genes with false discovery rates of <0.1 and fold change ≥2-fold were identified as differentially expressed genes. Functional annotations were assigned according to Alba et al. (2005).

Cellular Analysis

Determination of Plastid Parameters in Intact Cells

Tomato fruit tissues were harvested and fixed immediately in 3.5% (v/v) glutaraldehyde solution for 1 h in the dark (Cookson et al., 2003). Pericarp cells were prepared from green fruit by heating at 60°C for 15 min in a 0.1 M Na_2-EDTA solution and ripening fruit by storage in Na_2-EDTA at room temperature. Nomarski differential interference contrast optics on a Nikon Optiphot microscope in conjunction with Lucia image software were used to determine plastid parameters per cell. Total plastid area per cell and plastid number per cell were determined. Cell index parameters were calculated as a measure of the total plastid compartment size in relation to cell size, calculated as total plastid area per cell/cell plan area. The cell plan area is the area of the top view of the cell.

Tissue for electron microscopy was prepared from fruit derived from three plants of identical genotype. Pericarp tissue was fixed in 4% (v/v)

formaldehyde, 3% (v/v) glutaraldehyde buffered in 0.1 PIPES, pH 7.2, for 1.5 h at 4°C, and then rinsed in buffer. The same buffer containing 1% (w/v) OsO_4 was used to fix the tissues at 4°C overnight. Samples were repeatedly washed with aqueous ethanol (10 to 50% [v/v]) and finally dehydrated with ethanol washes. Embedding used Spurr's resin and sectioning was performed. Sections were stained with ethanol-saturated uranyl acetate and Reynold's lead stain. Transmission electron microscopy was performed on an EM109 (Zeiss).

Metabolite Analysis

Preparation of Tomato Tissue

The tomato fruit tissue used for metabolite analysis was derived from the same batch as that used for molecular analysis and thus prepared in an identical manner, with the exception that the material was freeze-dried. Metabolite analysis was performed on a minimum of three (up to six) biological replicates, with up to four technical replicates.

Carotenoid and Isoprenoid Analysis

The extraction, HPLC separation, photodiode array (PDA) detection, and quantification of carotenes, carotenoids, xanthophylls, tocopherols, and quinones has been described in detail previously (Fraser et al., 2000). A 10- to 20-mg aliquot of ground homogeneous fruit tissue was extracted with chloroform and methanol (2.5:1 by volume) after mixing and incubation for 20 min on ice, 1 volume of 100 mM Tris-HCl, pH 8.0, was added. A partition was formed after mixing by centrifugation. The organic hypophase was removed and the aqueous phase reextracted with chloroform (2.5 by volume). HPLC separations were performed using a C_{30} reverse-phase column (250 × 4.6 mm) purchased from YMC. The mobile phases used were methanol (A), water/methanol (20/80 by volume) containing 0.2% ammonium acetate (B), and *tert*-methyl butyl ether (C). The gradient used was 95% A:5% B, isocratically for 12 min and then stepped to 80% A:5% B:15% C from which a linear gradient to 30% A:5% B:65% C over 30 min was performed. A Waters Alliance model 2695 injection and solvent delivery system was used. Detection was performed continuously from 220 to 700 nm with an online PDA (Waters 966). Identification was performed by cochromatography and comparison of spectral properties with authentic standards and reference spectra (Britton, 2004). Annotated chromatograms of this HPLC system have been provided elsewhere (Fraser et al., 2007). Quantitative determination of carotenoids was performed by comparison with dose–response curves (0.2 to 1.0 μg) constructed from authentic standards. Purchasing, preparation, and characterization of authentic standards have been described previously (Fraser et al., 2000; Long et al., 2006). Total carotenoids along with chlorophyll A and B were determined spectrophotometrically as described by Wellburn (1994).

Flavonoids and Phenylpropanoid Analysis

Procedures used to extract, separate, detect, and quantify phenylpropanoids and flavonoids from freeze-dried tomato material have been detailed by Davuluri et al. (2005) and Long et al. (2006). Typically, 20 mg of freeze-dried powder (homogenized in the freezer mill as described earlier) was extracted with methanol (1 mL) containing salicylic acid as an internal standard (10 μg). The mixture was heated to 90°C for 60 min after cooling the suspension centrifuged at 3000*g* for 5 min the supernatant removed and extracts passed through a 0.2-μm syringe fitting filter before HPLC analysis. An Agilent 1100 HPLC solvent delivery system was used to separate phenylpropanoids and flavonoids on a reverse-phase C_{18} column (250 mm × 4.6 mm; 5 μm; Hichrom). The mobile phase consisted of (A) 2% water in methanol acidified with 0.015% HCl by volume and (B) acetonitrile. The initial gradient conditions used were 95% A, 5% B for 10 min, followed by a linear gradient to 50% B over 30 min. An online PDA enabled detection and identification from characteristic UV/Vis spectra. Authentic standards were used to confirm the identity of the phenylpropanoids and flavonoids. Relative quantification was carried out by comparison of integrated peak areas with the internal standard at the λmax of the phenylpropanoids and flavonoids detected. Total anthocyanins were extracted and quantified as described by Martin et al. (1985). Identification of the predominant anthocyanin was performed by liquid chromatography–electrospray ionization–mass spectrometry using identical conditions to those described above with the inclusion of formic acid instead of HCl in the mobile phase.

Phytosterol Analysis

Total phytosterols were routinely extracted from ground tomato powder prepared in the freezer mill as described above. β-Cholestanol was added as an internal standard (20 μg) and the suspension saponified with 5% KOH in 80% ethanol (5 mL) for 1 h at 90°C. When cooled, this solution was neutralized with concentrated sulphuric acid (~200 μL). The phytosterols were extracted with hexane (2 × 3 mL), adding water (5 mL) to create a partition. The pooled hexane extracts were dried under nitrogen and the residue redissolved in acetonitrile (20 μL) and derivatized by adding 20 μL *N*-methyltrimethylsilytrifluoroacetaminde (Sigma-Aldrich). This mixture was incubated at 37°C for 1 h. Separation and detection of phytosterols were performed with a Varian CP3380 gas chromatogram containing a flame ionization detector and fitted with an autosampler CP8410, and separation was performed on a CP-SIL8 column (Varian). The temperature program used consisted of 140°C initial conditions increasing to 240°C by 27 min at 4°C per min and holding for 2 min. These conditions were then held for another 18 min. The injector (Varian 1177) temperature was set at 260°C. Quantification was performed from integrated peak areas relative to a known amount of the internal standard.

Extraction, Derivatization, and Gas Chromatography–Mass Spectrometry Analysis of Metabolites

Methanol (1 mL; HPLC grade) and the internal standard ribitol (20 mg/mL) were added to freeze-dried (20 to 25 mg) tomato powder. The material and the suspension was mixed vigorously and then incubated at room temperature for 30 min with continuous agitation. To remove cell debris, samples were centrifuged at 12,000 rpm for 2 min, the resulting supernatant was removed, and from each sample an aliquot (100 μL) removed and dried completely under nitrogen gas. At this point, the extracts could be derivatized immediately or stored without degradation at −20°C. Derivatization was performed by the addition of 30 μL methoxyamine-HCl (Sigma-Aldrich) prepared at a concentration of 20 mg/mL in pyridine. After incubation in screw-capped tubes at 37°C for 2 h, *N*-methyltrimethylsilytrifluoroacetaminde from Macherey Nagel was added (85 μL) and the samples incubated for a further 1 h at 37°C before analysis. Gas chromatography–mass spectrometry analysis was performed on an Agilent HP6890 gas chromatograph with a 5973MSD. Typically, samples (1 μL) were injected with a split/splitless injector at 290°C with a 20:1 split and repeated on a 200:1 split for sugar quantification. Retention time locking to the internal standard was used. The gas chromatography oven was held for 4 min at 70°C before ramping at 5°C/min to 310°C. This final temperature was held for a further 10 min, making a total time of 60 min. The interface with the MS was set at 290°C and MS performed in full scan mode using 70 eV EI+ and scanned from 10 to 800 D. To identify chromatogram components found in the tomato profiles, a mass spectral (MS) library was constructed from in-house standards as well as the NIST 98 MS library. Chromatogram components were initially processed by the automated MS deconvolution and identification system. A retention time calibration was performed on all standards to facilitate the determination

of retention indices (RIs). Using the retention indices and MS, identification was performed by comparison with the MS library. Quantification was achieved using Chemstation (Agilent) software facilitating integrated peak areas for specific compound targets (qualifier ions) relative to the ribitol internal standard peak.

Total Antioxidant Activity Assays

A nonpolar extract was generated using the carotenoid/isoprenoid extraction procedure described above. The amount of homogenized freeze-dried tomato tissue used was 10 mg. Polar extracts were produced using the method described for phenylpropanoid and flavonoid extraction, with the exception that 90% aqueous methanol was used, no internal standard was added, the sample was not heated, and incubation time was extended to 2 h at room temperature in the dark. TEAC assays were performed as described by Re et al. (1999) by generating 2,2′-azinobis (3-ethylbenzothiazoline-6-sulphonic acid) (ABTS; purchased from Sigma-Aldrich), free radical cation, $ABTS^+$. To generate this reagent, an ABTS stock solution (7.0 mM) was mixed with 2.45 mM dipotassium peroxidisulfate (Sigma-Aldrich) in a 1:1 ratio. The mixture was left in the dark for 12 h at room temperature. This ABTS-free radical cation solution formed was diluted in ethanol, typically 8 μL $ABTS^+$ in ethanol (1 mL). An absorbance of 0.70 Abs at 734 nm should result. Sample (10 μL) was added to 1 mL $ABTS^+$ solution and the Abs 734 nm recorded. Results were compared with the ability of Trolox (a water-soluble vitamin E analog) to quench the $ABTS^+$ radical. Results were expressed as a TEAC in mmol of Trolox per gram of DW.

Data Processing and Statistical Treatment

All experimentation typically used a minimum of three biological and three technical replicates unless stated otherwise. Metabolite levels from the different technology platforms were combined. PCA analysis was performed on these data matrixes. SPSS software version 12.01 (SPSS) and SIMCA-P+ (Umetrics) were used to carry out and display clusters derived from PCA analysis. Student's *t* tests were used to determine significant differences between pairwise comparisons among the different *DET1* varieties with their control (T56). Where appropriate, $P < 0.05$, $P < 0.01$, and $P < 0.001$ are indicated by *, **, and ***, respectively. Student's *t* tests, means, and standard deviations were all calculated using GraphPad Prism software (GraphPad Software) or Excel (Microsoft) embedded algorithms. The overlaying of metabolite data over biochemical pathways was performed using BioSynLab software (www.biosynlab.com) from csv Excel files.

The mean and P values for 2A11, TFM7, and P119 transcriptome data sets were calculated from all the expression ratios including three biological and two technical replicates, each with a dye-swap, and redundant signals, and the unique transcripts having P values <0.05 were retained for the final analysis. Boxplot and frequency of distribution analysis was performed on a set of transcripts common to all developmental stages in both the P119 and TFM7 varieties, selected on the basis of P values (309 and 746 transcripts for P119 and TFM7, respectively). The boxplots, histograms, and multivariate analysis (CA and SOM) of gene expression data were performed within the R statistical programming environment (www.r-project.org) using packages MADE4 available from Bioconductor. The hierarchy of significantly affected pathways in transcriptomic data was established using Plant MetGenMap (Joung et al., 2009). For each transcriptome analysis, the plate IDs available for the entire set of transcripts data with P value <0.05 has been usd. The software uses hypergeometric test to check the significance of pathway changes, performed on a set of pathways simultaneously using P values that correspond to raw P values corrected by false discovery rate. Unprocessed microarray data are available at www.mycib.ac.uk/zope/TomSysBio.

Correlation analysis between metabolites and transcripts (variables) was performed by calculating Pearson's correlation coefficients. BioSynLab (www.biosynlab.com) and MATLAB (www.mathworks.com) software programs were used to calculate correlation coefficients. A P value <0.05 was used to judge the significance of the correlation coefficients. Positive and negative correlations have been represented as heat maps using a false color scaling. To obtain greater robustness of significance correlation analysis, data sets for all the *DET1* genotypes have been used with triplicate biological replication per genotype. Transcripts common to all varieties used in the analysis have been provided in Supplemental Data Set 1 online.

Accession Numbers

The microarray and metabolomic data sets are available through the Biotechnology and Biological Science Research Council (BBSRC) Centre for Plant Integrative Biology at www.mycib.ac.uk/zope/TomSysBio. The accession numbers and properties of the genes used in microarray and correlation analysis are provided in Supplemental Data Set 1 online. Supplemental Table 6 online contains the accession numbers for the genes used in qRT-PCR analysis.

Supplemental Data

The following materials are available in the online version of this article.

Supplemental Figure 1. Determination of Both Lipophilic and Hydrophilic Antioxidant Activity in Both Mature Green and Ripe Fruit.

Supplemental Figure 2. Altered Plastid Parameters Resulting from the *hp2^j* Mutant Allele.

Supplemental Figure 3. Changes in Metabolites Occurring in Mature Green and Ripe Fruit as a Result of *DET1* Downregulation under the Control of the TFM7 Promoter.

Supplemental Figure 4. Changes in Metabolites Occurring in Mature Green and Ripe Fruit as a Result of *DET1* Downregulation under the Control of the 2A11 Promoter.

Supplemental Figure 5. Correspondence Analysis for P119 and TFM7.

Supplemental Figure 6. Overview of Relative Changes in Gene Expression.

Supplemental Figure 7. Heat Map Illustrating the Changes Occurring in Gene-to-Gene Correlations Resulting from *DET1* Downregulation at the Mature Green Stage of Fruit Development.

Supplemental Figure 8. Heat Map Illustrating the Changes Occurring in Gene-to-Gene Correlations Resulting from *DET1* Downregulation at the Stage of Ripe Fruit.

Supplemental Figure 9. Heat Map Illustrating the Changes Occurring in Gene-to-Gene Correlations Resulting from *DET1* Downregulation at the Mature Green Stage of Fruit Development.

Supplemental Figure 10. Heat Map Illustrating the Changes Occurring in Gene-to-Gene Correlations Resulting from *DET1* Downregulation at the Ripe Stage of Fruit Development.

Supplemental Figure 11. Heat Map Displaying Transcript and Metabolite Correlations Associated with the Relative Changes Resulting from *DET1* Downregulation Compared with the Wild-Type (T56) Control at the Mature Green Fruit Developmental Stage, and the Ripe Fruit Stage, as well as an Analysis of Correlations between Mature Green Transcripts and Ripe Fruit Metabolites.

Supplemental Table 1. The Stability of the Increased Carotenoid Phenotype in *DET1* Lines over the T3 to T5 Generations.

Supplemental Table 2. Metabolite Levels of *DET1* Varieties Relative to Their Respective Controls at the Mature Green and Ripe Fruit Stages.

Supplemental Table 3. Changes in Relative Metabolite Levels Found in *DET1* Varieties during Fruit Development and Ripening.

Supplemental Table 4. Overview of Global Changes in P119 and TFM7 Transcript Levels during Ripening.

Supplemental Table 5. Hierarchy of Pathways Significantly Affected in P119 and TFM7 *DET1* Varieties.

Supplemental Table 6. Primer Sequences used for Quantitative Real-Time RT-PCR and PCR.

Supplemental Data Set 1. Gene Identifiers for Transcripts Used in Correlation Analysis.

ACKNOWLEDGMENTS

This work was supported in part by EU-FP6 EU-SOL to P.M.B., P.D.F., and C.B., a PhD studentship from ANR-07-BLAN-0216 from the French Agence Nationale de la Recherche to I.A., long-term fellowship LT00299/2005 from the Human Frontier Science Program to F.B., ANR-BBSRC SysBio BB/F005644/1 to P.M.B., P.D.F., and C.B., Agronanotech Fondo per gli Investimenti della Ricerca di Base and GenoPom from Ministero dell'Istruzione, dell'Università e della Ricerca to C.B., and EU-FP7 METAPRO 244348 to P.D.F. The tomato microarray expression profiling analysis was supported by the USDA–Agricultural Research Service and Grant 0501778 and 0606595 from the National Science Foundation Plant Genome Research Program to J.J.G. We thank Tom Wells for bioinformatic assistance and help, John Halket for assistance with metabolomic analysis, and Gita Patel and Marta Staff for assistance in gathering cellular data. P.D.F. and E.M.A.E. also thank Lee Sweetlove for valuable discussions and advice on aspects of primary metabolism. We thank the TGRC for the supply of *hp* mutant seeds.

Received January 5, 2010; revised March 23, 2010; accepted April 6, 2010; published April 30, 2010.

REFERENCES

Alba, R., et al. (2004). ESTs, cDNA microarrays and gene expression profiling: tools for dissecting plant physiology and development. Plant J. **39:** 697–714.

Alba, R., Payton, P., Fei, Z., McQuinn, R., Debbie, P., Martin, G., Tanksley, S., and Giovannoni, J. (2005). Transcriptome and selected fruit metabolite analysis reveal multiple points of ethylene regulatory control during tomato fruit development. Plant Cell **17:** 2954–2965.

Aldridge, C., Maple, J., and Moller, S.G. (2005). The molecular biology of plastid division in higher plants. J. Exp. Bot. **56:** 1061–1077.

Allan, A.C., Hellens, R.P., and Laing, W.A. (2008). MYB transcription factors that colour our fruit. Trends Plant Sci. **13:** 99–102.

Apel, W., and Bock, R. (2009). Enhancement of carotenoid biosynthesis in transplastomic tomatoes by induced lycopene to Provitamin A conversion. Plant Physiol. **151:** 59–66.

Benvenuto, G., Formiggini, F., Laflamme, P., Malakhov, M., and Bowler, C. (2002). The photomorphogenesis regulator DET1 binds the amino-terminal tail of histone H2B in a nucleosome context. Curr. Biol. **12:** 1529–1534.

Britton, G. (2004). Carotenoids Handbook. (Basel, Switzerland: Birkhäuser-Verlag).

Butelli, E., Titta, L., Giorgio, M., Mock, H.-P., Matros, A., Peterek, S., Schijlen, E.G.W.M., Hall, R.D., Bovy, A.G., Luo, J., and Martin, C.A. (2008). Enrichment of tomato fruit with health-promoting anthocyanins by expression of select transcription factors. Nat. Biotechnol. **26:** 1301–1308.

Chory, J., and Peto, C.A. (1990). Mutations in the *DET1* gene affect cell-type-specific expression of light-regulated genes and chloroplast development in *Arabidopsis.* Proc. Natl. Acad. Sci. USA **87:** 8776–8780.

Chory, J., Peto, C.A., Feinbaum, R., Pratt, L., and Ausubel, F. (1989). *Arabidopsis thaliana* mutant that develops as a light-grown plant in the absence of light. Cell **58:** 991–999.

Cominelli, E., Gusmaroli, G., Allgera, D., Galbiati, M., Wade, H.K., Jenkins, G.I., and Tonelli, C. (2008). Expression analysis of anthocyanin regulatory genes in response to different light qualities in *Arabidopsis thaliana.* J. Plant Physiol. **165:** 886–894.

Cookson, P.J., Kiano, J.W., Shipton, C.A., Fraser, P.D., Roemer, S., Schuch, W., Bramley, P.M., and Pyke, K.A. (2003). Increases in cell elongation, plastid compartment size and phytoene synthase activity underlie the phenotype of the high pigment-1 mutant of tomato. Planta **217:** 896–903.

Cooper, D.A. (2004). Carotenoids in health and disease: Recent scientific evaluations, research recommendations and the consumer. J. Nutr. **134:** 221–224.

Davuluri, G.R., Tuinen, A., Mustilli, A.C., Manfredonia, A., Newman, R., Burgess, D., Brummell, D.A., King, S.R., Palys, J., Uhlig, J., Pennings, H.M.J., and Bowler, C. (2004). Manipulation of DET1 expression in tomato results in photomorphogenic phenotypes caused by post-transcriptional gene silencing. Plant J. **40:** 344–354.

Davuluri, G.R., et al. (2005). Fruit-specific RNAi-mediated suppression of DET1 enhances tomato nutritional quality. Nat. Biotechnol. **23:** 890–895.

Diretto, G., Al-Babili, S., Tavazza, R., Papacchioli, V., Beyer, P., and Giuliano, G. (2007). Metabolic engineering of potato carotenoid content through tuber-specific overexpression of a bacterial mini-pathway. PLoS One **2:** e350.

Fitter, D.W., Martin, D.J., Copley, M., Scotland, R.W., and Langdale, J.A. (2002). GLK gene pairs regulate chloroplast development in diverse plant species. Plant J. **31:** 713–727.

Foo, E., Ross, J.J., Davies, N.W., Ried, J.B., and Weller, J.L. (2006). A role for ethylene in the phytochrome-mediated control of vegetative development. Plant J. **46:** 911–921.

Foyer, C.H., and Noctor, G. (2005). Redox homeostasis and antioxidant signaling: A metabolic interface between stress perception and physiological responses. Plant Cell **17:** 1866–1877.

Fraser, P.D., Enfissi, E.M.A., and Bramley, P.M. (2009). Genetic engineering of carotenoid formation in tomato fruit and the potential application of systems and synthetic biology approaches. Arch. Biochem. Biophys. **482:** 196–204.

Fraser, P.D., Enfissi, E.M.A., Halket, J.H., Truesdale, M.R., Yu, D.M., Gerrish, C., and Bramley, P.M. (2007). Manipulation of phytoene levels in tomato fruit: Effects on isoprenoids, plastids and intermediary metabolism. Plant Cell **19:** 3194–3211.

Fraser, P.D., Pinto, M.E., Holloway, D.E., and Bramley, P.M. (2000). Application of high-performance liquid chromatography with photodiode array detection to the metabolite profiling of plant isoprenoids. Plant J. **24:** 551–558.

Fraser, P.D., Roemer, S., Shipton, C.A., Mills, P.B., Kiano, J.W., Misawa, N., Drake, R.G., Schuch, W., and Bramley, P.M. (2002). Evaluation of transgenic tomato plants expressing an additional phytoene synthase in a fruit-specific manner. Proc. Natl. Acad. Sci. USA **99:** 1092–1097.

Galpaz, N., Wang, Q., Menda, N., Zamir, D., and Hirschberg, J.

(2008). Abscisic acid deficiency in the tomato mutant high-pigment3 leading to increased plastid number and higher fruit lycopene content. Plant J. **53:** 717–730.

Ghassemian, M., Lutes, J., Tepperman, J.M., Chang, H.-S., Zhu, T., Wang, X., Quail, P.H., and Lange, M.B. (2006). Integrative analysis of transcript and metabolite profiling data sets to evaluate the regulation of biochemical pathways during photomorphogenesis. Arch. Biochem. Biophys. **448:** 45–59.

Giliberto, L., Perrotta, G., Weller, J.L., Fraser, P.D., Bramley, P.M., Fiore, A., Tavazza, M., and Giuliano, G. (2005). Manipulation of the blue light photoreceptor cryptochrome2 in tomato affects vegetative development, flowering time and fruit antioxidant content. Plant Physiol. **137:** 199–208.

Gillaspy, G., Ben-David, H., and Gruissem, W. (1993). Fruits: A developmental perspective. Plant Cell **5:** 1439–1451.

Giovannoni, J. (2004). Genetic regulation of fruit development and ripening. Plant Cell **16:** S170–S180.

Giovannucci, E. (2002). Lycopene and prostate cancer risk. Methodological considerations in the epidemiologic literature. Pure Appl. Chem. **74:** 1427–1434.

Grant, G.R., Liu, J., and Stoeckert, C.J., Jr. (2005). A practical false discovery rate approach to identifying patterns of differential expression in microarray data. Bioinformatics **11:** 2684–2690.

Griffiths, A., Barry, C.S., Alpuche-Solils, A., and Grierson, D. (1999). Ethylene and developmental signals regulate expression of lipoxygenase genes during tomato fruit ripening. J. Exp. Bot. **50:** 793–798.

He, K., Stolc, V., Lee, H., Figueroa, P., Gao, Y., Tongprasit, W., Zhao, H., Lee, I., and Deng, X.W. (2007). Analysis of transcription factor HY5 genomic binding sites revealed its hierarchical role in light regulation of development. Plant Cell **19:** 731–749.

Huq, E., Tepperman, J.M., and Quail, P. (2000). GIGANTEA is a nuclear protein involved in phytochrome signalling in *Arabidopsis.* Proc. Natl. Acad. Sci. USA **97:** 9789–9794.

Joung, J.-G., Corbett, A.M., Moore-Fellman, S., Tieman, D.M., Klee, H.J., Giovannoni, J.J., and Fei, Z. (2009). Plant MetGenMAP: An integrative analysis system for plant systems biology. Plant Physiol. **151:** 1758–1768.

Jung, S. (2004). Effect of chlorophyll reduction in *Arabidopsis thaliana* by methyl jasmonate or norflurazon on antioxidant systems. Plant Physiol. Biochem. **42:** 225–231.

Key, T.J., Allen, N.E., Spencer, E.A., and Travis, R.C. (2002). The effect of diet on risk of cancer. Lancet **360:** 861–868.

Kolotilin, I., Koltai, H., Tadmor, Y., Bar-Or, C., Reuveni, M., Meir, A., Nahon, S., Shlomo, H., Chen, L., and Levin, I. (2007). *Transcriptional* profiling of high pigment-2^{dg} tomato mutant links early plastid biogenesis with its overproduction of phytonutrients. Plant Physiol. **145:** 389–401.

Liu, Y., Roof, S., Ye, Z., Barry, C., van Tuinen, A., Verbalov, J., Bowler, C., and Giovannoni, J. (2004). Manipulation of light signal transduction as a means of modifying fruit nutritional quality in tomato. Proc. Natl. Acad. Sci. USA **101:** 9897–9902.

Long, M., Millar, D.J., Kimura, Y., Donovan, G., Rees, J., Fraser, P.D., Bramley, P.M., and Bolwell, G.P. (2006). Metabolite profiling of carotenoid and phenolic pathways in mutant and transgenic lines of tomato: Identification of a high antioxidant fruit line. Phytochemistry **67:** 1750–1757.

Lopez-Juez, E., Dillon, E., Magyar, Z., Khan, S., Hazeldine, S., de Pager, S.M., Murria, J.A.H., Beemster, G.T.S., Bogre, L., and Shanahan, H. (2008). Distinct light-initiated gene expression and cell cycle programs in the shoot apex and cotyledons of *Arabidopsis.* Plant Cell **20:** 947–968.

Luo, J., Butelli, E., Hill, L., Parr, A., Niggeweg, R., Bailey, P., Weisshaar, B., and Martin, C.A. (2008). AtMYB12 regulates caffeoyl quinic acid and flavonol synthesis in tomato: Expression in fruit results in very high levels of both types of polyphenol. Plant J. **56:** 316–326.

Ma, L., Li, J., Qu, L., Hager, J., Chen, Z., Zhao, H., and Deng, X.W. (2001). Light control of *Arabidopsis* development entails coordinated regulation of genome expression and cellular pathways. Plant Cell **13:** 2589–2607.

Ma, L., Zhao, H., and Deng, X.W. (2003). Analysis of the mutational effects of the COP/DET/FUS loci on genome expression profiles reveals their overlapping yet not identical roles in regulating *Arabidopsis* seedling development. Development **130:** 969–981.

Maass, D., Arango, J., Wüst, F., Beyer, P., and Welsch, R. (2009). Carotenoid crystal formation in *Arabidopsis* and carrot roots caused by increased phytoene synthase protein levels. PLoS One **4:** e6373.

Martin, C., Carpenter, R., Sommer, H., Saedler, H., and Coen, E.S. (1985). Molecular analysis of instability in flower pigmentation of *Antirrhinum majus*, following isolation of the pallida locus by transposon tagging. EMBO J. **4:** 1625–1630.

Muir, S.R., Collins, G.J., Robinson, S., Hughes, S., Bovy, A., De Vos, C.H.S., van Tunen, A.J., and Verhoeyen, M.E. (2001). Overexpression of petunia chalcone isomerase in tomato results in fruit containing increased levels of flavonols. Nat. Biotechnol. **19:** 470–474.

Naqvi, S., Zhu, C., Farre, G., Ramessar, K., Bassie, L., Breitenbach, J., Perez-Conesa, D., Ros, G., Sandmann, G., Capell, T., and Christou, P. (2009). Transgenic multivitamin corn through biofortification of endosperm with three vitamins representing three distinct metabolic pathways. Proc. Natl. Acad. Sci. USA **106:** 7762–7767.

Osterlund, M.T., Hardtke, C.S., Wei, N., and Deng, X.W. (2000). Targeted destabilization of HY5 during light-regulated development of *Arabidopsis.* Nature **405:** 462–466.

Re, R., Pellergrini, N., Protrggente, A., Pannala, A., Yang, M., and Rice-Evans, C.A. (1999). Antioxidant activity applying an improved ABTS radical cation decolorization assay. Free Radic. Biol. Med. **26:** 1231–1237.

Sasaki-Sekimoto, Y., et al. (2005). Coordinated activation of metabolic pathways for antioxidants and defence compounds by jasmonates and their roles in stress tolerance in *Arabidopsis.* Plant J. **44:** 653–668.

Schäfer, E., and Bowler, C. (2002). Phytochrome-mediated photoperception and signal transduction in higher plants. EMBO Rep. **3:** 1042–1048.

Schroeder, D.F., Gahrtz, M., Maxwell, B.B., Cook, R.K., Kan, J.M., Alonso, J.M., Ecker, J.R., and Chory, J. (2002). De-etiolated 1 and damaged DNA binding protein 1 interact to regulate *Arabidopsis* photomorphogenesis. Curr. Biol. **12:** 1462–1472.

Terzaghi, W., and Cashmore, A. (1995). Light-regulated transcription. Annu. Rev. Plant Physiol. Plant Mol. Biol. **46:** 445–474.

Triques, K., Sturbios, B., Gallais, S., Dalmais, M., Chauvin, S., Clepet, C., Aubourg, S., Rameau, C., Caboche, M., and Bendahmane, A. (2007). Characterisation of *Arabidopsis* thaliana mismatch specific endonucleases: application to mutation discovery by TILLING in pea. Plant J. **51:** 1116–1125.

Vanderauwera, S., Zimmermann, P., Rombauts, S., Vandenabeele, S., Langebartels, C., Gruissem, W., Inze, D., and Van Breusegem, F. (2005). Genome-wide analysis of hydrogen peroxide-regulated gene expression in *Arabidopsis* reveals a high light-induced transcriptional cluster involved in anthocyanin biosynthesis. Plant Physiol. **139:** 806–821.

Verhoeyen, M.E., Bovy, A., Collins, G., Robinson, S., De Vos, C.H.R., and Colliver, S. (2002). Increasing antioxidant levels in tomatoes through modification of the flavonoid biosynthetic pathway. J. Exp. Bot. **53:** 2099–2106.

Wang, S.H., Liu, J.K., Feng, Y.Y., Niu, X.L., Giovannoni, J., and Liu, Y.S. (2008). Altered plastid levels and potential for improved fruit

content by down-regulation of the tomato DDB1-interacting protein CUL4. Plant J. **55:** 89–103.

Wasternack, C. (2006). Jasmonates; An update on biosynthesis, signal transduction and action in plant stress response, growth and development. Ann. Bot. (Lond.) **100:** 681–697.

Wei, H., Persson, S., Mehta, T., Srinivasasainagendra, V., Chen, L., Page, G.P., Somerville, C.R., and Loraine, A. (2006). Transcriptional coordination of the metabolic network in *Arabidopsis.* Plant Physiol. **142:** 762–774.

Wellburn, A.R. (1994). The spectral determination of chlorophyll A and chlorophyll B as well as total carotenoids, using various solvents and with spectrophotomers of different resolution. J. Plant Physiol. **144:** 307–313.

Yang, Y.H., Dudoit, S., Luu, P., Lin, D.M., Peng, V., Ngai, J., and Speed, T.P. (2002). Normalisation for cDNA microarray data: A robust composite method addressing single and multiple slide systematic variation. Nucleic Acids Res. **30:** e15.

Yasumura, Y., Moylan, E.C., and Langdale, J.A. (2005). A conserved transcription factor mediates nuclear control of organelle biogenesis in anciently diverged land plants. Plant Cell **17:** 1894–1907.

Ye, X.D., Al-Babili, S., Kloti, S., Zhang, J., Lucca, P., Beyer, P., and Potrykus, I. (2000). Engineering the provitamin A (beta-carotene) biosynthetic pathway into (carotenoid-free) rice endosperm. Science **287:** 303–305.

Youssef, A., Laizet, Y., Block, M.A., Marechal, E., Alcaraz, J.-P., Larson, T.R., Pontier, D., Gaffe, J., and Kuntz, M. (2009). Plant lipid-associated fibrillin proteins condition jasmonate production under photosynthetic stress. Plant J. **61:** 436–445.

Zamir, D. (2001). Improving plant breeding with exotic genetic libraries. Nat. Rev. Genet. **2:** 983–989.